MASTER THESIS

FLUID STRUCTURE INTERACTION USING REDUCED ORDER MODELS - A FIRST APPROACH

ALEXIS TELLO GUERRA

ADVISORS:

RAMON CODINA

JOAN BAIGES

ESCOLA TÈCNICA SUPERIOR D'ENGINYERS DE CAMINS, CANALS I PORTS DE BARCELONA

UNIVERSITAT POLITÈCNICA DE CALATUNYA

CONTENTS

LIST OF FIGURES

List of Figures

ACKNOWLEDGMENTS

This is just the beginning of the journey towards what I hope to be perfect understanding of many, many things. Or in other words my PH.D, acknowledgments will be longer in that moment.

I would like to thank my advisors, Ramon Codina and Joan Baiges, for their patience until now, and for sharing their knowledge with me.

To Ernesto Castillo, because thanks to his advise many of the results here shown were possible.

To Ricardo Reyes with whom apparently anything can be programmed.

To Judyta, the reason everything makes sense.

1 INTRODUCTION

Since the moment humans started to manipulate their surroundings to acommodate to their daily lives engineering became part of it as well. Humanity has come a long way since then, and now priority has shifted from the 'what to build' to 'how to build it' with the evolution of engineering and optimization driving every day life. A change that has not been driven by anything else than the need to reduce costs and understand mistakes. And what would be of a decent fluid structure interaction themed project with out mention of the Tacoma bridge, the cornerstone of modern era design failure.

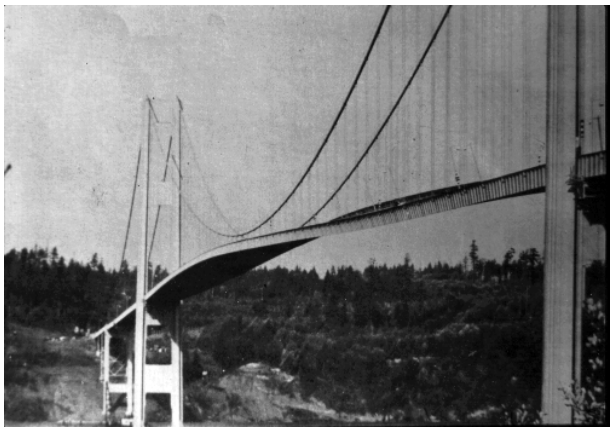

Figure 1.1: Tacoma bridge oscillating before its collapse

In figure 1.1 the Tacoma bridge can be seen oscillating seconds before its collapse into the river. At the moment not much was understood about what caused its demise but surprisingly this proved to change the way dynamic processes were

seen and a new field of engineering was created, one in which the interaction between fluid and solid were centerline.

On the other hand this change of paradigm into and optimization driven one was further promoted with the advent of computation and cost reduction of material processes. From the possibility to solve linear systems progressively faster, reduced order modeling is born out of a necessity and a desire to save that which humans are always running out of, time.

The underlying idea idea in ROM is to further increase the abstraction of any kind of numerical system and treat it as any kind of data. This will be decomposed into the most energetic modes and then use this as a way to recreate the same, or similar processes. Much like a Fourier transform does to a dynamic process.

This project investigates in a more experimental fashion the collision between the two areas, Fluid Structe Interaction and Reduced Order Modeling and is developed in a progessive manner, first benchmarking each particular physics and then attempting to replicate the obtained results by use of ROM.

In this order of ideas firstly a review of the theory behind solid elasticity and navierstokes equations is made with the respective benchmarking of the code. Then a review of the fluid structure interaction problem from the mathematical point of view is made to be able to finally study FSI with a common test case. Finally a quick view of the theory behind reduced order models is done to conclude with applications to solid dynamics, fluid flow and finally FSI.

It is the hope of the author that with this project a methodology can be understood as to how to study FSI and then make progress into ROM analysis. This project is the initial part of what will become a doctoral thesis in the same frame of research.

During the development of this master thesis project several tasks have been undergone, from coding a linear solid elasticity module in the code used by the

research group, see chapter 6, re design of key features in the same code to be able to study coupling between physical modules and by this be able to produce FSI cases and application of previously coded algorithms to develop and understand fluid flow and ROM.

2 LINEAR ELASTICITY

Linear elasticity, despite being a simplification of the general theory of elasticity, has been proved to provide exact, or nearly so, results to a broad range of engineering problems. All the results presented in this paper have been obtained by applying this theory. Hence it is worthwhile to have a look at the underlying assumptions and its range of application.

The main assumptions under which linear elasticity is based upon are infinitesimal strains and the existence of a neutral state. The first one means that there is no distintion between the material and spatial tensors, which by getting rid of the nonlinear part, collapses into the symmetric infinitesimal strain tensor.

If the strains are denoted by ϵ and the displacements by $\mathbf{d}$, the relation between these two variables is given by,

$$\boldsymbol{\epsilon} = \bigtriangledown^{s}\mathbf{d} \tag{2–1}$$

On the other hand, for the second assumption the neutral state is generally understood as the initial configuration, or configuration of reference.

$$\begin{aligned} \boldsymbol{\epsilon}(\mathbf{x}, \mathbf{t}_0) &= 0 \\ \boldsymbol{\sigma}(\mathbf{x}, \mathbf{t}_0) &= 0 \end{aligned} \tag{2–2}$$

The next step is defining a relationship between stresses and strains. As in most solid elasticity applications, it is desired to know what happens when certain stress is applied to a given mechanical part, or on the contrary, what kind of stress will this part undergo when deformed a certain amount. This relationship is called Hook's law and states that there exists a linear relationship between stress and strain shown in 2–3.

$$\boldsymbol{\sigma}(\mathbf{x}, \mathbf{t}) = C\boldsymbol{\epsilon}(\mathbf{x}, \mathbf{t}) \tag{2–3}$$

Where C is a fourth order tensor known as the elastic tensor.

Variational problem and discretization

For a certain domain Ω with boundary $\partial\Omega$ and $]0, T[$ the interval of analysis the elastodynamic problem consists in finding a displacement $\mathbf{u}$ such that:

$$\rho\partial_{tt}^2\mathbf{d} - \nabla\cdot\boldsymbol{\sigma} = \rho\mathbf{f} \text{ in } \Omega, t \in]0, t[\tag{2–4}$$

$$\tag{2–5}$$

$$\mathbf{d} = 0 \text{ On } \Gamma_D, \tag{2–6}$$

$$\mathbf{n}\cdot\boldsymbol{\sigma} = \mathbf{t} \text{ On } \Gamma_N, \tag{2–7}$$

$$\tag{2–8}$$

Where $\mathbf{C}$ is elasticity tensor, $\mathbf{f}$ is the force vector and $\mathbf{t}$ is a prescribed traction on the boundary of the domain. It must be noted that when dealing with one dimensional problems the elasticity tensor collapses to a quantity known as Young's modulus E.

To proceed with the solution of this set of equations its important first to define some notation that will make the problem more manageable.

The space of functions whose p power ($p \geqslant 1$) is integrable in a domain ω is denoted by $L^p(\omega)$, and the space of functions whose distributional derivatives of order up to $m \geqslant 0$ belong to $L^2(\omega)$ by $H^m(\omega)$. The space $H_0^1(\omega)$ consists of functions in $H^1(\omega)$ vanishing on the domain boundary $\partial\omega$. The topological dual of $H^1(\omega)$ is denoted by $H^{-1}(\Omega)$, and the duality pairing by $\langle\cdot,\cdot\rangle$. A bold character denotes a vector counterpart of these spaces. The L^2 inner product in ω for scalars, vectors or tensors is denoted by $(\cdot,\cdot)_\omega$, and the norm in the Banach space X by $\|\cdot\|_X$. This notation is simplified in some cases as follows: $(\cdot,\cdot)_\Omega \equiv (\cdot,\cdot), \|\cdot\|_{L^2(\Omega)} \equiv \|\cdot\|$ and if K is the domain of an element $\|\cdot\|_{L^2(K)} \equiv \|\cdot\|_K$.

Using this notation the displacements belongs to the following finite element space, $\mathscr{W} = \mathbf{e} \in \mathbf{H}^1(\Omega)^d | \mathbf{e} = 0$ on Γ_D.

Now multiplying against a test function v and integrating by parts we define a a bilinear form B and a linear form L as,

$$\mathbf{B}(\mathbf{d},\mathbf{e}) = (\mathbf{C} : \nabla^S \mathbf{d}, \nabla^S \mathbf{e})_\Omega \tag{2–9}$$

and,

$$L(\mathbf{e}) = \langle \mathbf{f}, \mathbf{e} \rangle_\Omega \tag{2–10}$$

with appropriate initial conditions at $t = 0$.

Spatial discretization

For the spatial discretization the standard Galerkin finite elements approximation can be defined as follows. Let $\mathcal{P}_h$ denote a finite element partition of the domain Ω. The diamater of an element domain $K \in \mathcal{P}$ is denoted by h_k and the diameterof the finite element partition by $h = max\{h_k | K \in \mathcal{P}\}$. We can now construct conforming

finite element spaces $\mathscr{W}_h \subset \mathscr{W}$ as well as the corresponding subspace $\mathscr{W}_{h,0}$. Then the problem can be written as,

$$\rho(\partial_{tt}\mathbf{u}, \mathbf{e}) + \mathbf{B}(\mathbf{d}_h, \mathbf{e}_h) = L(\mathbf{e}_h), \forall \mathbf{e}_h \in \mathscr{W}_{h,0} \tag{2–11}$$

Unless otherwise noted bilinear quadrilateral elements were used for all cases.

Time discretization

In FSI stationary problems are rarely a case of interest as many of the variables involved evolve through time. In this sense it is obvious that the best of efforts in achieving a good spatial discretization and the posterior solution is worthless if the solution can not be carried in time with similar or better precision.

All solutions were obtained by means of the Newmark time integration scheme, which is of the following form,

$$\mathbf{v}_{n+1} = \mathbf{v}_n + \Delta t \left[\gamma \mathbf{a}_n + \gamma \mathbf{a}_n + 1\right] \tag{2–12}$$

$$\mathbf{x}_{n+1} = \mathbf{x}_n + \Delta t \mathbf{v}_n + \frac{\Delta t}{2} \left[(1 - 2\beta)\mathbf{a}_n + 2\beta \mathbf{a}_n + 1\right] \tag{2–13}$$

Where $\mathbf{x}_{n+1}$, $\mathbf{v}_{n+1}$ and $\mathbf{a}_{n+1}$ are approximations to the position, velocity and acceleration vectors at a determined time step n. β and γ are parameters that define the method and are of particular interest with value of $1/4$ and $1/2$ respectively, which assumes that the acceleration over the time step is constant and equal to $(\mathbf{a}_n - \mathbf{a}_{n+1})/2$, reason by which it is also called 'Constant acceleration method',[10], most importantly it has degree of accuracy of order two and that it is non dissipative, reason why methods like BDF1 and BDF2 were not considered.

The only inconvenience of this method is the need to store additional information like the velocities and accelerations where the primary unknown are the positions for different time intervals. On the other hand, this can be beneficial when dealing with FSI problems where the solid is non linear and thus can affect flow behavior, this calculated velocity can be passed to the solid as dirichlet conditions instead of a prescribed mesh movement, this is not explored in this work but is left as a short term objective. This set of equations can be treated implicitly but all solid dynamic cases were run by explicitly solving these quantities.

2.1 BENCHMARKING

The process of Benchmarking any code, or piece of it, is a fundamental step of code validation. With the aim of succesfully solving fluid structure interaction problems two benchmarks have been produced for a linear elastic problem. The first one dealing with the stationary results of a beam under effect of a distributed load and the second one with the dynamic response of a common geometry undergoing free vibration.

2.1.1 Stationary problem - Plain strain cook's membrane

The Cook's membrane problem is a common benchmark for validating element formulations. The problem consists of a tapered beam which is clamped on one side and free on the other. The free side undergoes a shear force P.

The general set up of the case is shown in figure 2.1.

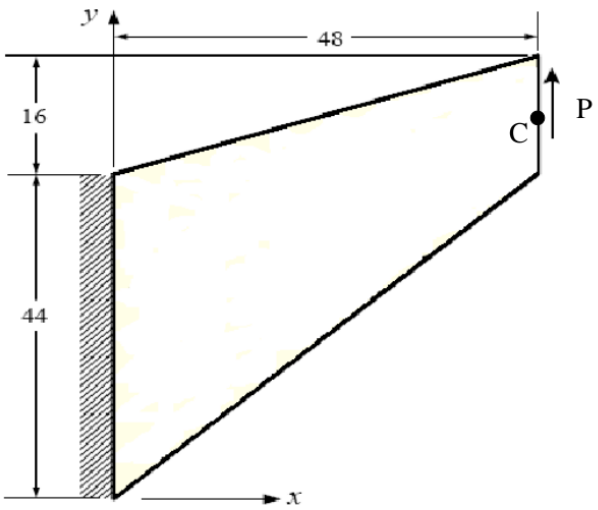

Figure 2.1: Diagram of Cook's problem [11]

Mesh, Numerical and Physical parameters

Figure 2.2 shows an example of the meshes used. In this case bi-linear quadrilaterals and linear triangles are compared for increasing elements on the geometry's side.

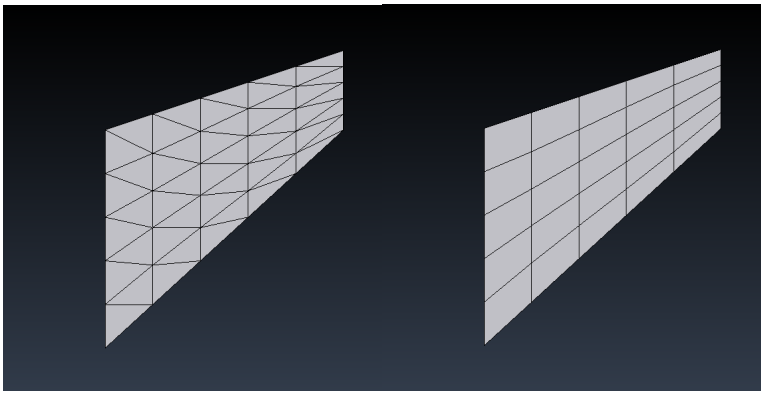

(a) Triangular **(b)** Quadrilaterals

Figure 2.2: Example of 5 elements per side

All cases were run for the following physical properties and numerical parameters:

Young's modulus	1
Poisson's modulus	$\frac{1}{3}$
Shear force	1

Results

Results shown in figure 2.3 show a slightly improved convergence for triangular elements compared to quadrilaterals for displacement of point C under the mentioned load. Beyond the 30 element limit convergence for both elements is almost identical.

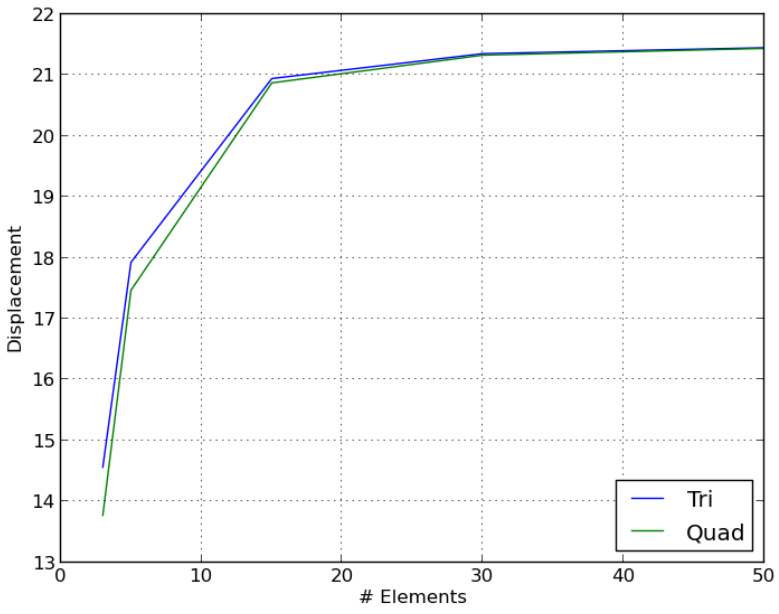

Figure 2.3: Displacement for triangles and quadrilaterals

A convergence plot is shown in 2.4

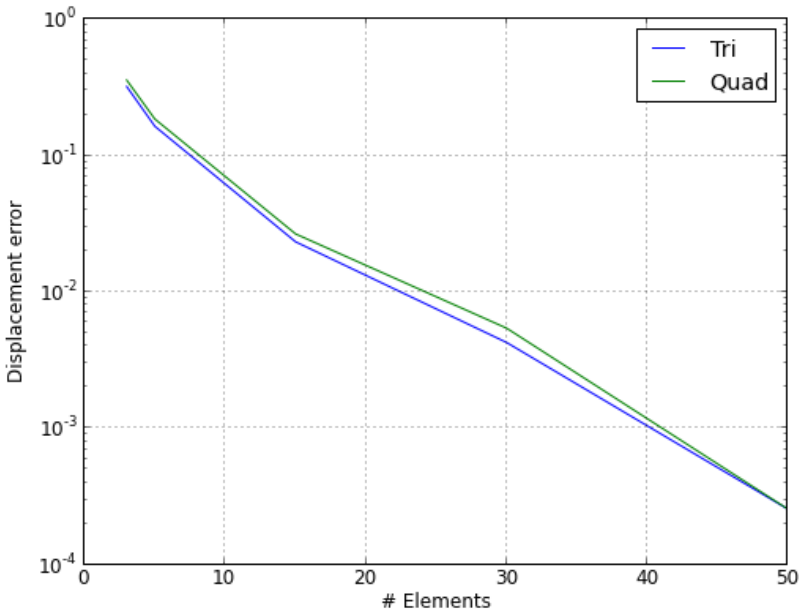

Figure 2.4: Convergence for triangles and quadrilaterals

Obtained results are in agreement with the behavior seen in [3], although the case was run with different parameters, and are almost identical to the results shown in [11] in which the same case was run.

A Poisson of 0.5 the produces element locking in which non feasible results are obtained, this is expected near the incompressible limit for the used elements.

2.1.2 Dynamic problem - Oscillating bar

The validation of the dynamic problem is of critical importance on the solution of fluid structure interaction problems. The methodology consisted on reproducing a problem that could be solved by both analytical and numerical ways. The oscillation of a bar with various boundary conditions has been extensively studied and its development can be found in most structural dynamic or vibration textbooks

like [10]. For the present case the the configuration of a clamped-free end bar was selected.

Its analytical solution can be found by the following equation:

$$\omega_n = \alpha \left(\frac{EI}{\rho L^4} \right)^{\frac{1}{2}} \tag{2–14}$$

Where α is equal to 3.52 for the first mode of vibration and to 22 for the second one. From this the theoretical first and second modes of vibration for the present problem are found to be:

ω_1	40.815 Hz
ω_2	259.731 Hz

Mesh, Numerical and Physical parameters

Figure 2.5 shows an example of the meshes used, as in the previous benchmark, linear triangles and bi-linear quadrilaterals were used for all cases.

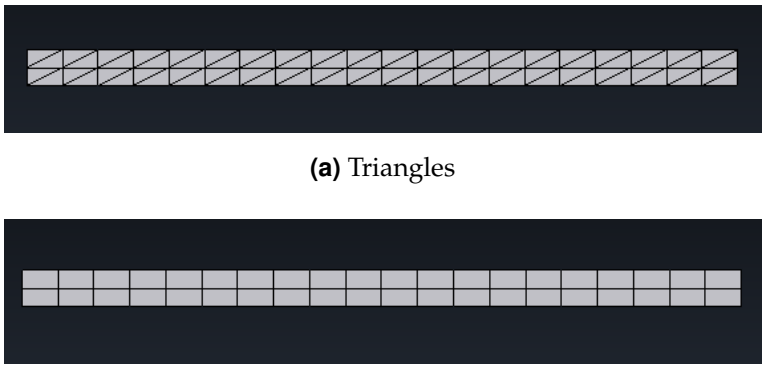

(a) Triangles

(b) Quadrilaterals

Figure 2.5: Example of 2X20 mesh

The following table shows the numerical and physical parameters used for all cases run.

Young's modulus	$200e^9$
Poisson's modulus	$\frac{1}{3}$
Density	7810
time step	$1e^{-5}$
total time	1

Time integration and Fourier transform

The time integration was done by means of the Newmark constant acceleration method, other time integration schemes like the BDF1 and BDF2 produced too much numerical damping. Point tracking was used in the middle section of the free end. After solution a discrete Fourier transform was done to the obtained data. A sample of the obtained spectrum is shown in figure 2.6 showing the first and second harmonics of the geometry where both the first and second harmonics can be seen to be quite close to their theoretical value.

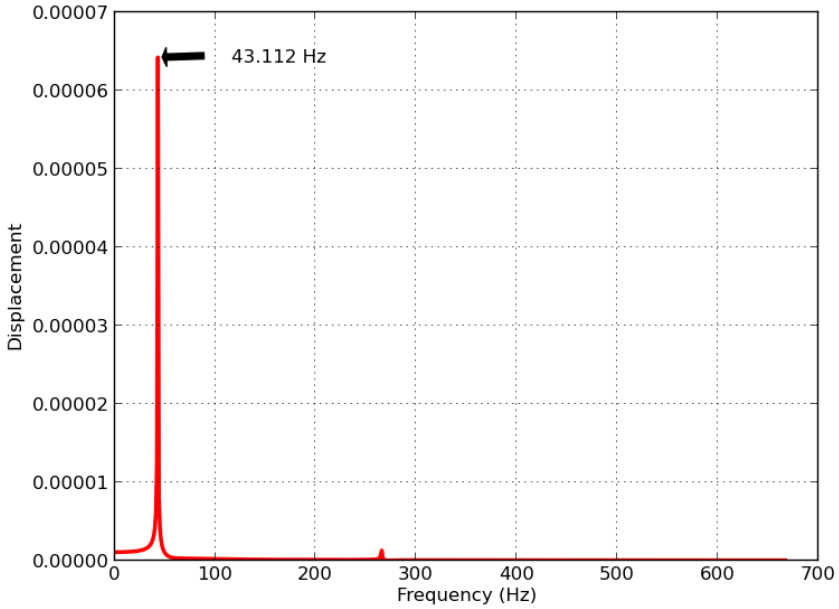

Figure 2.6: dFt of a case run

Convergence for various test cases is shown in the following section.

Results

Figure 2.7 shows the convergence for linear triangles and bi-linear quadrilaterals for incremental number of elements for the first harmonic or natural mode of vibration of the bar. The theoretical value is shown as a red continous line.

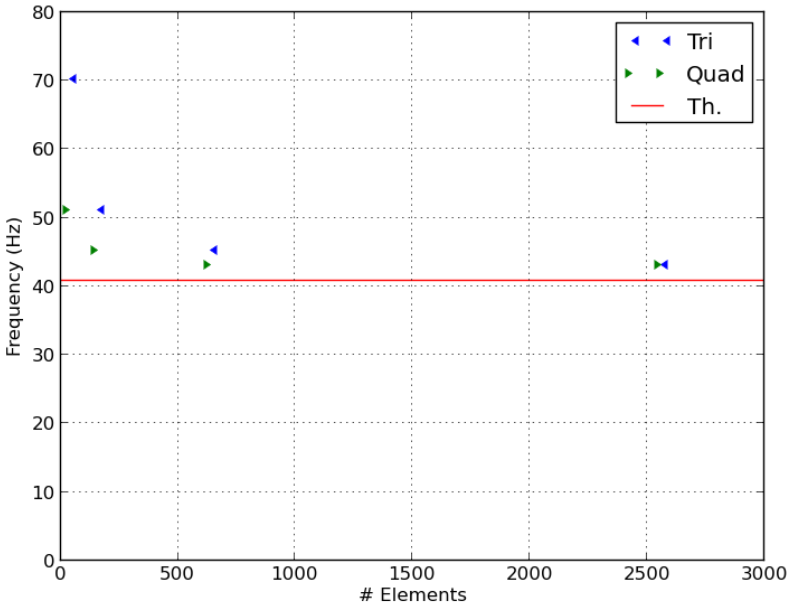

Figure 2.7: Convergence for triangles and quadrilaterals

As it can be seen, for a low number of elements the frequency is found to be much higher than its expected value converging in a rapid manner as the number of elements is increased. In this case quadrilaterals exhibit an improved convergence when compared to triangles.

Results are close to the theoretical value, the difference is atributed to the bending of the perpendicular planes along the beam's geometry as the theory does not take this into account, coming from the Euler-Bernoulli approximation. Results were found to be the same for any number of elements on the beam thickness. One factor that was found to improve convergence in quadrilaterals to the theoretical value was reducing the poisson modulus to zero, on the other hand this did not help for linear triangles.

3 INCOMPRESSIBLE NAVIER-STOKES EQUATIONS

Once linear elasticity has been reviewed the last step before dealing with FSI problems is dealing with fluid dynamics. In this section a short review of the necessary theory and some test cases are explained. For a certain domain Ω with boundary $\partial\Omega$ and $]0, T[$ the interval of analysis the Navier-Stokes problem consists in finding a velocity $\mathbf{u}$ and pressure p such that:

$$\begin{aligned} \partial_t \mathbf{u} - \nu \triangle \mathbf{u} + \mathbf{u} \cdot \nabla \mathbf{u} + \nabla p = \mathbf{f} \text{ in } \Omega, \ t \in]0, t[\\ \nabla \cdot \mathbf{u} = 0 \text{ in } \Omega, \ t \in]0, t[\end{aligned} \tag{3–1}$$

Where ν is the kinematic viscosity and $\mathbf{f}$ is the force vector.

Using the notation defined in chapter 2, the velocity and pressure finite element spaces are $\mathscr{V}_0 := \mathbf{H}_0^1(\Omega)$, $\mathscr{Q} := L^2(\Omega)/\mathbb{R}$, $\mathscr{X}_0 := \mathscr{V}_0 \times \mathscr{Q}_0$.

Now if we define a a bilinear form B and a linear form L as,

$$B = \nu(\nabla \mathbf{u}, \nabla \boldsymbol{\nu}) + (\mathbf{u} \cdot \nabla \mathbf{u}, \boldsymbol{\nu}) - (p, \nabla \cdot \boldsymbol{\nu}) + (q, \nabla \cdot \mathbf{u}) \tag{3–2}$$

and,

$$L = \langle \mathbf{f}, \nu \rangle \tag{3–3}$$

The variational form of the Navier-Stokes equations can be written as,

Find $[u, p] \in \mathbf{L}^2(0, T; \mathscr{V}_0) \times \mathbf{L}^1(0, T; Q_0(\Gamma))$ such that

$$\partial_t \mathbf{u} + \mathbf{B}(\mathbf{U}, \mathbf{V}) = L(\mathbf{V}), \forall\ \mathbf{V}\ \in\ \mathscr{X}_0 \tag{3–4}$$

For $\mathbf{U} \equiv [\mathbf{u}, \mathbf{p}] \in \mathscr{X}_0$ and $\mathbf{V} \equiv [\boldsymbol{\nu}, \mathbf{q}] \in \mathscr{X}_0$. Where initial and boundary conditions should hold.

A feasible solution for this problem will be found depending on the Babuska-Brezzi, defined in equation 3–5, condition which basically states that a suitable interpolating space for velocity and pressure must be found. From this it can be understood that the choice of elements cannot be random and why it is not possible to use the same kind of element for both variables.

$$\inf \sup \frac{q_h, \nabla \cdot \boldsymbol{\nu}_h}{\|q_h\| \|\boldsymbol{\nu}_h\|_1} \geqslant \beta > 0, \tag{3–5}$$

for constant β independent of h.

SPATIAL DISCRETIZATION

For the spatial discretization the standard Galerkin finite elements approximation can be defined as follows. Let $\mathcal{P}_h$ denote a finite element partition of the domain Ω. The diamater of an element domain $K \in \mathcal{P}$ is denoted by h_k and the diameter of the finite element partition by $h = max\{h_k | K \in \mathcal{P}\}$. We can now construct conforming finite element spaces $\mathscr{V}_h \subset \mathscr{V}$, $\mathscr{Q}_h \subset \mathscr{Q}$ and $\mathscr{X}_h = \mathscr{V}_h \times \mathscr{Q}_h$ as well as the corresponding subspaces $\mathscr{V}_{h,0}$,$\mathscr{Q}_{h,0}$ and $\mathscr{X}_h = \mathscr{V}_{h,0} \times \mathscr{Q}_{h,0}$. Then the problem can be written as,

Find $\mathbf{U}_h \in \mathscr{X}_{h,0}$

$$\partial_t \mathbf{u} + \mathbf{B}(\mathbf{U}_h, \mathbf{V}_h) = L(V_h), \forall\, \mathbf{V}_h \in \mathscr{X}_{h,0} \tag{3–6}$$

TIME DISCRETIZATION

For the temporal discretization the usual finite differences scheme is adopted. In particular the Backward Euler (BE) or Backward Differences schemes, in particular BDF1 and BDF2 that are of the form:

$$\frac{\partial \mathbf{u}_h^{j+1}}{\partial t} = \frac{\mathbf{u}^{j+1} - \mathbf{u}^j}{\Delta t} + O(\Delta t) \tag{3–7}$$

$$\frac{\partial \mathbf{u}_h^{j+1}}{\partial t} = \frac{3\mathbf{u}^{j+1} - 4\mathbf{u}^j + \mathbf{u}^{j-1}}{\Delta t} + O(\Delta t^2) \tag{3–8}$$

After initial trial runs BDF1 was found to be too dissipative and BDF2 became the default time integration algorithm for all fluid flow cases.

SUBGRID SCALES

To deal with the stability issues associated to the different spaces to where velocity and pressure belong, stabilized versions of equation 3–6 have been developed in which the bilinear form B is replaced with a mesh dependent version B_h.

On the other hand, when the problem is convection dominated spurius oscillations may appear that propagate and possibly explode accross the time advance. To handle this situations stabilized upwind schemes have been developed where

the residual is used as an additional diffusive term. All cases shown in this work rely on this basic concept.

The idea is to divide the problem in two parts, the first one being the one that can be solved as ussual by means of the normal FEM approximation over the defined grid. The second one being the one that approximates what cannot be solved directly of over the grid, or in other words, the sub grid. Though simple and intuitive this idea is fairly recent and, when developed proved to be groundbraking as it opened a whole new frontier for numerical approximation of highly convective flows.

This formulations are based on the Variational Multiscale Method proposed by Hughes on [8], and ,as mentioned, the idea is to approximate the space $\mathscr{X}$ as a composition of the grid and subgrid spaces as $\mathscr{X} = \mathscr{X}_h \oplus \widetilde{\mathscr{X}}$. Where $\widetilde{\mathscr{X}}$ is the space of subscales. This leads to the following modified continous version of the Navier-Stokes problem,

$$\partial_t \mathbf{u} + \mathbf{B}(\mathbf{U}_h, \mathbf{V}_h) + \mathbf{B}(\widetilde{\mathbf{U}}_h, \mathbf{V}_h) = L(V_h), \forall\, \mathbf{V}_h \in \mathscr{X}_{h,0} \tag{3–9}$$

$$\partial_t \mathbf{u} + \mathbf{B}(\mathbf{U}_h, \widetilde{\mathbf{V}}_h) + \mathbf{B}(\widetilde{\mathbf{U}}_h, \widetilde{\mathbf{V}}_h) = L(V_h), \forall\, \widetilde{\mathbf{V}}_h \in \widetilde{\mathscr{X}_0} \tag{3–10}$$

Integrating by parts within each element equations 3–9 and 3–10 can be written as,

$$\begin{aligned} &(\partial_t \mathbf{u}, \mathbf{v}) + \mathbf{B}(\mathbf{U}_h, \mathbf{V}_h) + \sum_K \int_K \widetilde{\mathbf{U}} \cdot \mathscr{L}^*(\mathbf{V}_h) d\Omega + \\ &\sum_K \int_{\partial K} \widetilde{\mathbf{u}} \cdot (q_h \mathbf{n} + \nu \mathbf{n} \cdot \nabla \boldsymbol{\nu}_h) d\Gamma = L(V_h),\ \forall\, \mathbf{V}_h \end{aligned} \tag{3–11}$$

$$(\partial_t \mathbf{u}, \mathbf{v}) + \sum_K \int_K \widetilde{\mathbf{V}} \cdot \mathscr{L}(\widetilde{\mathbf{U}}) d\Gamma + \sum_K \int_{\partial K} \widetilde{\mathbf{v}} \cdot (p_h \mathbf{n} + \nu \mathbf{n} \cdot \nabla \mathbf{u}_h) d\Gamma = \sum_K \int_K \widetilde{\mathbf{V}} \cdot [\mathbf{F} - \mathscr{L}(\mathbf{U}_h] d\Omega, \tag{3–12}$$

Where $\mathscr{L}^*$ is the formal adjoint of the linear operator and has the form,

$$\mathscr{L}^*(\mathbf{V}_h) = \begin{bmatrix} -\nu \Delta \boldsymbol{v}_h - \mathbf{a} \cdot \nabla \boldsymbol{v}_h - \nabla q_h \\ -\nabla \cdot \boldsymbol{v}_h \end{bmatrix}$$

If tractions are continous across element boundaries the first term of equation 3–11 cancels out which leads to,

$\mathscr{L}(\widetilde{\mathbf{U}}) = \mathbf{R} := \mathbf{F} - \mathscr{L}(\mathbf{U}) + \mathbf{V}_{h,ort}$ in $K \in \mathcal{P}_h$, $\mathbf{V}_{h,ort} \in \widetilde{\mathscr{X}_0^{\perp}}$, where the main idea then is to approximate,

$$\widetilde{\mathbf{U}} \approx \boldsymbol{\tau}_K \mathbf{R} \tag{3–13}$$

Where τ_K is a matrix of parameters, denoted as the matrix of stabilization parameters, depending on K and the coefficients of the operator $\mathscr{L}$ and is the most important aspect of stabilized finite element methods. For all applications in the project τ_K is of the form,

$$\tau = \left(c_1 \frac{\nu}{h^2} + \sigma \right)^{-1} + \left(c_2 \frac{|\mathbf{a}|}{h} \right)^{-1} \tag{3–14}$$

For further detail see [4, 5]. During all of this development nothing was said about the time dependence of the subgrid part. As it turns out they can also be found to depend on time, but this is a more complex analysis and goes outside of the scope of this project, for further detail see [6].

4 FLUID STRUCTURE INTERACTION

After a quick review of solid elasticity and fluid flow the interaction between these two can be analyzed. In mathematical terms this is called an heterogeneous problem as two different systems of equations are interacting through certain coupling. In this sense it is worthwhile to review the underlying theory of interaction between subdomains to then advance to FSI.

4.1 THE HETEROGENEOUS PROBLEM [1]

Let Ω be the domain composed by two boundaries Γ_1 and Γ_2 as in figure 4.1

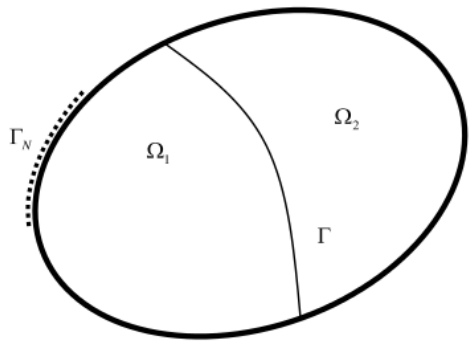

Figure 4.1: Partitioned domain, taken from [1]

The problem to be solved is the following,

$$
\begin{aligned}
\rho_S \partial_{tt}^2 \mathbf{d} - \nabla \cdot \boldsymbol{\sigma}_S &= \rho_S \mathbf{f} \text{ in } \Omega_S, \\
\mathbf{d} &= 0 \text{ On } \Gamma_{D_s}, \\
\mathbf{n}_s \cdot \boldsymbol{\sigma}_S &= \mathbf{f}_S \text{ On } \Gamma_{N_s}, \\
\rho_F \partial_{tt}^2 \mathbf{u} - \mu \Delta \mathbf{u} + \nabla p &= \rho_F \mathbf{f} \text{ in } \Omega_F, \\
\nabla \cdot \mathbf{u} &= 0 \text{ On } \Gamma_F, \\
\mathbf{u} &= 0 \text{ On } \Gamma_{D_F}, \\
-p\mathbf{n}_F + \mu \mathbf{n}_F \cdot \nabla \mathbf{u} &= \mathbf{t}_F \text{ On } \Gamma_{N_F}, \\
\mathbf{n}_s \boldsymbol{\sigma}_S + (-p\mathbf{n}_F + \mu \mathbf{n}_F \cdot \nabla \mathbf{u}) &= 0 \text{ On } \Gamma, \\
\partial_t \mathbf{d} - \mathbf{u} &= 0 \text{ On } \Gamma,
\end{aligned}
$$

Together with initial conditions for $\mathbf{u}$, $\mathbf{d}$ and $\partial_t \mathbf{d}$ in each respective domain. In variational form the problem can be stated as,

$$
\begin{aligned}
\rho_S(\partial_{tt}^2 \mathbf{d}, \mathbf{e})_{\Omega_S} + B_S(\mathbf{d}, \mathbf{e}) = L_S(\mathbf{e}) + \langle \mathbf{t_S}, \mathbf{e} \rangle_{\Gamma_{N_s}}, \ \forall \mathbf{e} \in \mathscr{W}, \\
\rho_F(\partial_t \mathbf{u}, \mathbf{v})_{\Omega_S} + B_F([\mathbf{u}, p], [\mathbf{v}, q]) = L_F([\mathbf{v}, q]) + \langle \mathbf{t_F}, \mathbf{v} \rangle_{\Gamma_{N_F}}, \ \forall [\mathbf{v}, q] \in \mathscr{V} \times \mathscr{Q}, \\
\langle \boldsymbol{\mu}, \partial_t \mathbf{d} - \mathbf{u} \rangle_\Gamma = 0 \in \boldsymbol{\mu}
\end{aligned}
$$

Where the spaces $\mathscr{W}, \mathscr{V}, \mathscr{Q}$ have been defined previously in chapters 2 and 3.

4.2 DISCRETE PROBLEM [1]

The discrete version of the fluid structure heterogeneous problem solved in a monolithic manner is given as follows,

$$\rho_S(D_{tt}\mathbf{d}_h^n, \mathbf{e}_h)_{\Omega_S} + B_S(\mathbf{d}_h^n, \mathbf{e}_h) = L_S(\mathbf{e}_h) + \langle \mathbf{t}_{SF}, \mathbf{e}_h \rangle \tag{4–1}$$

$$\rho_F(D_t\mathbf{u}_h^n, \mathbf{v}_h)_{\Omega_F} + B_{F,stab}([\mathbf{u}_h^n, \mathbf{p}_h^n], [\mathbf{v}_h, \mathbf{q}_h]) = L_{F,stab}([\mathbf{v}_h, \mathbf{q}_h]) + \langle \mathbf{t}_{SF}, \mathbf{v}_h \rangle \tag{4–2}$$

It is worth noticing that a monolithic approach can be very expensive to solve and specially to assemble, this is why in this project an iteration by subdomain approach was taken which has the following form,

$$\rho_S(D_{tt}\mathbf{d}_h^{n,i}, \mathbf{e}_h)_{\Omega_S} + B_S(\mathbf{d}_h^{n,i}, \mathbf{e}_h) = L_S(\mathbf{e}_h) - \mathcal{T}_F([\mathbf{u}_h^{n,i-1}, \mathbf{p}_h^{n,i-1}]) \tag{4–3}$$

$$\rho_F(D_t\mathbf{u}_h^{n,i}, \mathbf{v}_h)_{\Omega_F} + B_{F,stab}([\mathbf{u}_h^{n,i}, \mathbf{p}_h^{n,i}], [\mathbf{v}_h, \mathbf{q}_h]) = L_{F,stab}([\mathbf{v}_h, \mathbf{q}_h]) \tag{4–4}$$

Where it can be seen how the second term on the right hand side of the first equation is the one responsible for ensuring continuity between tractions between solid and fluid when tested against the displacement test function.

4.3 BENCHMARKING

While the process of benchmarking solid elasticity or fluid flow can be achieved in relatively simple cases in FSI this is not the case as there are specific restrictions in each domain. A case was chosen in which the flow around a cylinder with

a beam attached to it. The flow generates vortices that through traction initiate and mantain a state of oscillation in the beam. This test is known as the turek case and is ussually solved for non linear elasticity in which the beam deflection is quite large and in turn can affect the fluid flow. This case is quite suitable for ALE formulations as the mesh for the fluid domain moves to reproduce the solid deformation, see [7] for the full description of the experiment. In this case, due to time constraints the case was only analyzed for linear elasticity in which strains are small, which means that while the solid motion is driven by fluid coupling, the fluid is not affected by the solid motion.

Turek case

A diagram of the case is shown in figure 4.2 with definition of important parameters and variables.

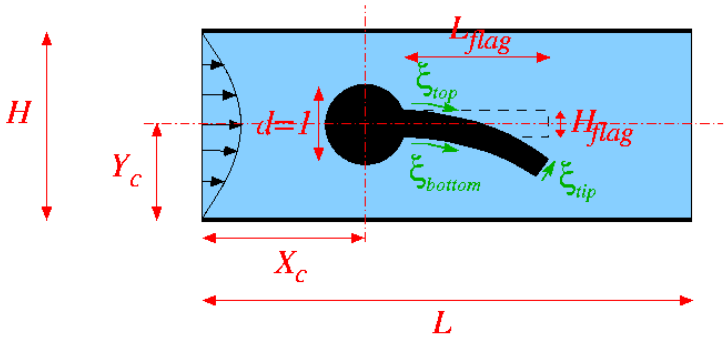

Figure 4.2: Description of the case, taken from [9]

Where the parameters have the values shown in table 4.1 for the cases run,

Cylinder diameter	$d = 1$
Center of cylinder	$X_c = Y_c = 2.0$
Channel length	$L = 25.0$
Thickness of undeformed beam	$H_{flag} = 0.2$
Right end of undeformed beam	$x_{tip} = 6.0$
Density of fluid	1
Viscosity of fluid	0.0025
Beam Young modulus	200e7
Beam density	7850
Beam Poisson	0.3

Table 4.1: Material properties and parameter of case

Figure 4.3 shows the actual geometry that was used. As the domain is large this inevitably means that the mesh for the fluid domain will be composed by a large number of elements, specially where the interface between solid and fluid exists.

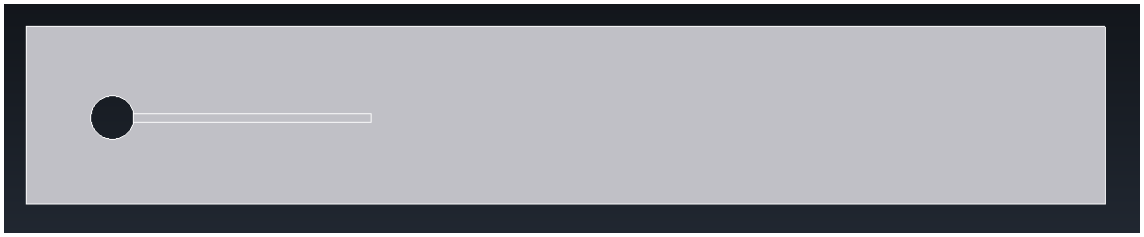

Figure 4.3: Geometry of the case

Table 4.2 shows the boundary conditions for the case.

Domain	Fluid	Solid
$x = 0$	$vel_x = 1, vel_y = 0.0$	
$x = 25$	$vel_x = vel_y = \text{Free}$	
$y = 0 = 4$	$vel_x = free, vel_y = 0$	
cylinder surface	$vel_x = vel_y = 0$	
beam surface	$vel_x = vel_y = 0$	$t_f = t_s$
cylinder beam union		$disp_x = disp_y = 0$

Table 4.2: Mesh properties for both domains

Mesh

Important sections of the mesh are shown in the following figures. Figure 4.4 shows the mesh over the cylinder and part of the beam. For a correct solution of the tractions over the beam it is necessary to correctly approximate the boundary layer that the fluid forms over it, which required mesh refinement over the elements in the interface.

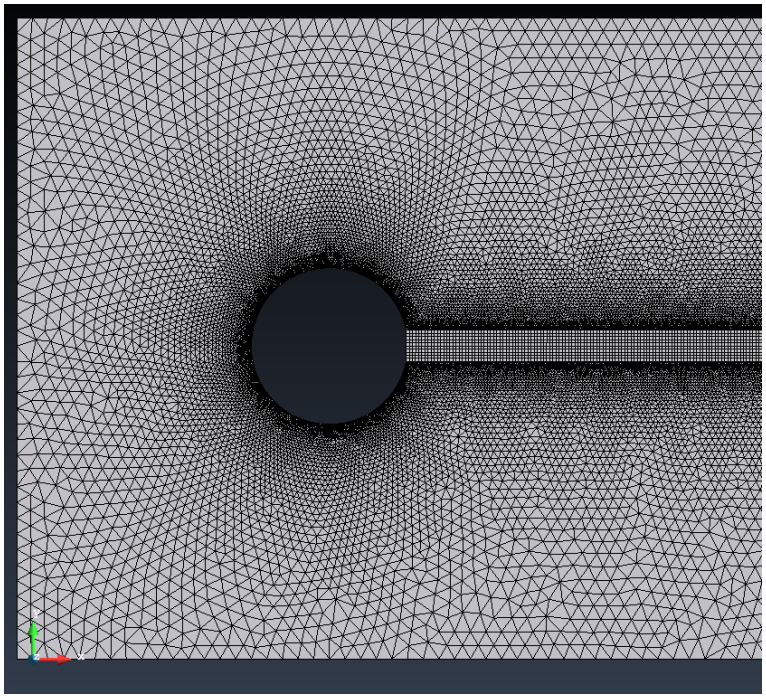

Figure 4.4: Mesh of fraction of domain

Figure 4.5 shows a close up of the mesh over the cylinder and a fraction of the beam. It is clear by now that the mesh of the cylinder and that of the fluid are non matching and most importantly, composed by different kind of elements. The fluid domain is composed by linear triangles while the beam is composed by bilinear quadrilaterals. This was chosen in this way for the fluid because triangles allow more versatility in terms of geometry reproduction and refinement over boundary layers. For the solid, as the physics are much simpler, a coarser mesh could be used that could be solved quickly and correctly. Moreover the fact that it is symmetric structured made the meshing process straightforward and produces more precise results, as was seen from the solid dynamic benchmarking process.

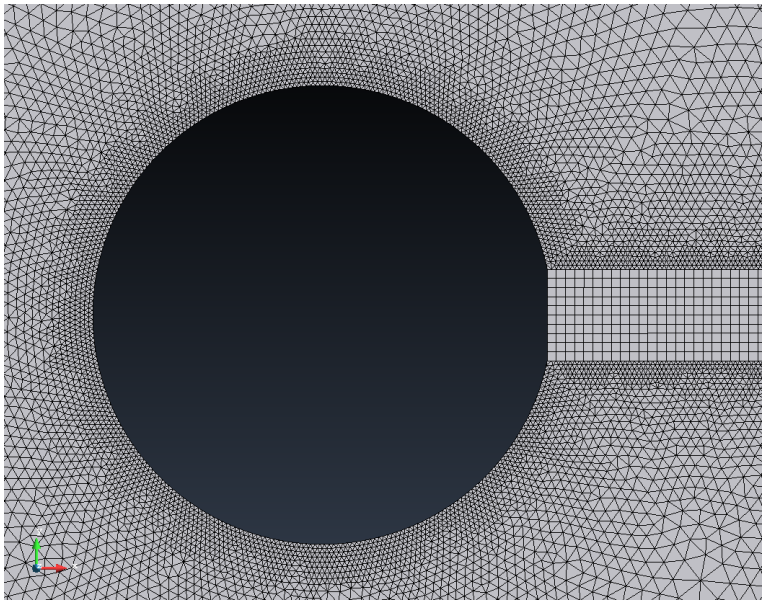

Figure 4.5: Mesh of the sphere

Finally figure 4.6 shows a close up of the mesh over the tip of the beam. Its worth noting, once again, that the mesh of the boundary layer is much denser that that of the beam. The issue of non conforming meshes could and was solved by used of a mesh to mesh interpolator that was introduced into the code just in time to make part of this project, see chapter 6 for more details.

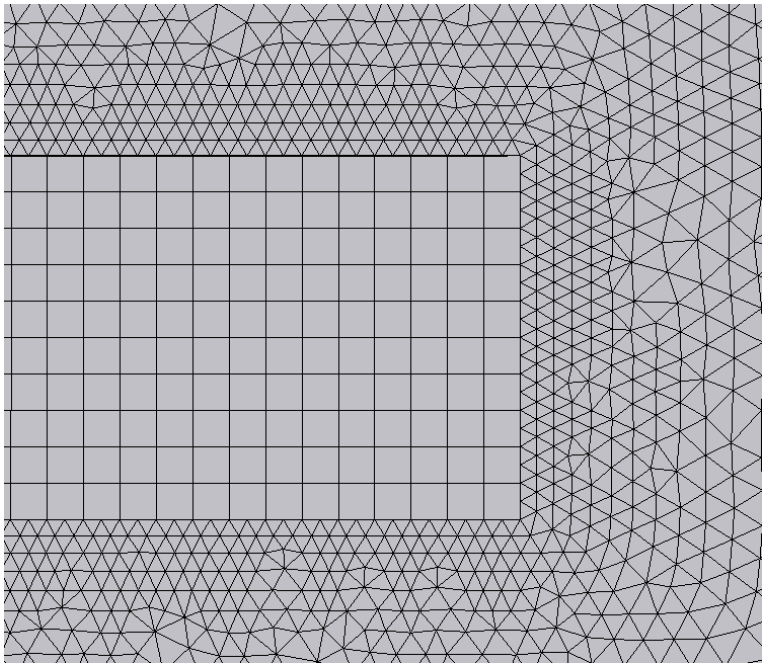

Figure 4.6: Mesh of tip of cantiliver beam

Table 4.3 shows important mesh parameters.

Domain	Fluid	Solid
Element	Linear Tri	Bilinear Quad
# Elements	65906	2760
# Nodes	33952	9134

Table 4.3: Mesh properties for both domains

Results

It was seen that for this particular problem the solution (velocity and pressure) had a period of oscillation of around 20 seconds so it was decided to run the case for 60 seconds with a time step of 0.05 seconds to be able to analyze at least three full periods of the solution, this is also important in next sections when ROM is

analyzed to be able to capture the lower modes of the fluids solution.

Results are displayed fro the fluid as contour plots for velocity and pressure and for the solid as point tracking for the tip of the beam attached to the cylinder. The motion of the tip is compared to the velocity of the fluid near it.

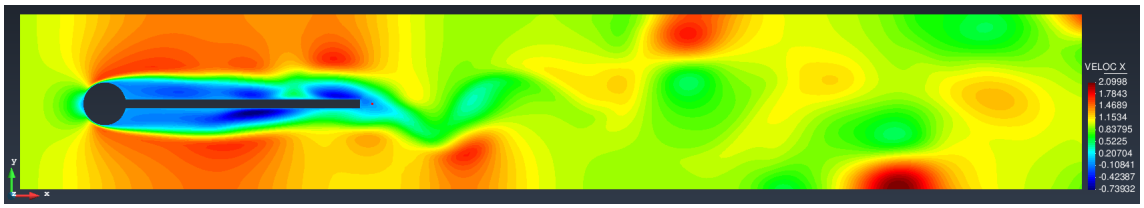

(a)

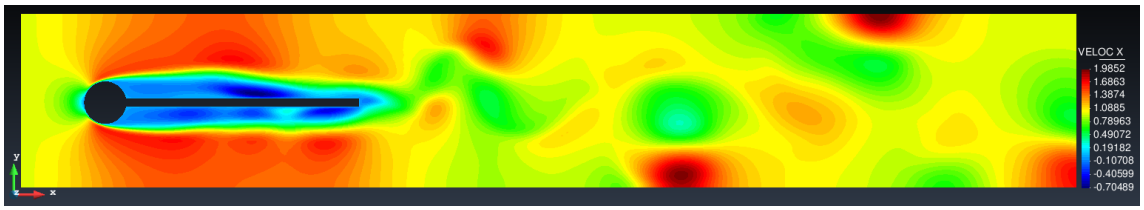

(b)

Figure 4.7: x velocity component, figure 4.7a shedding upper vortex, figure 4.7b shedding lower vortex

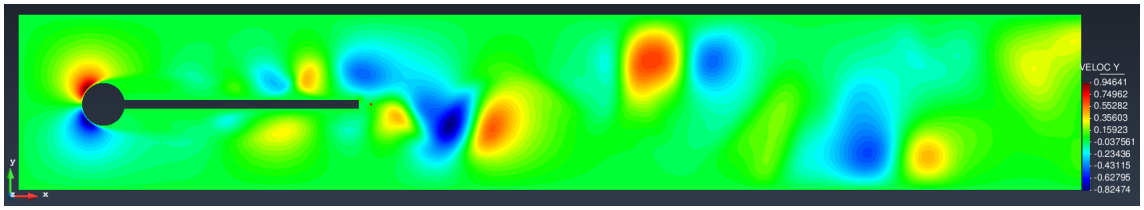

(a)

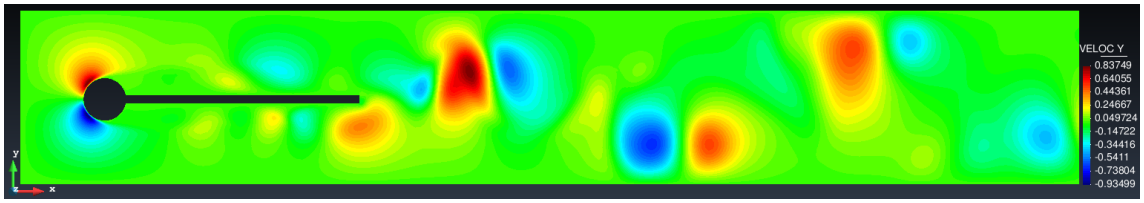

(b)

Figure 4.8: y velocity component, figure 4.8a shedding upper vortex, figure 4.8b shedding lower vortex

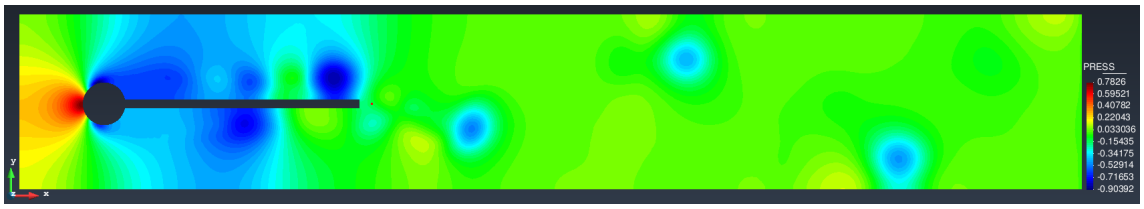

(a)

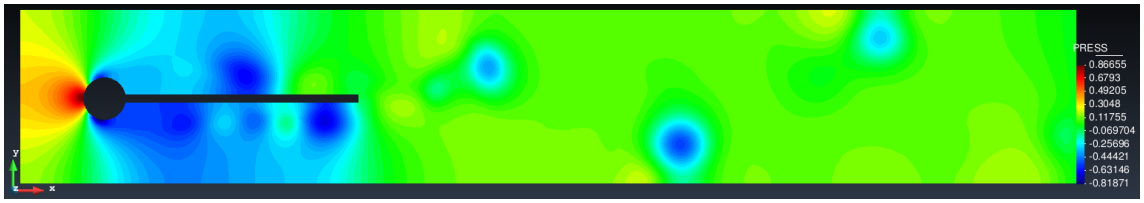

(b)

Figure 4.9: Pressure contours, figure 4.9a shedding upper vortex, figure 4.9b shedding lower vortex

It is intended to appreciate the oscillating nature of the solved quantities which has an evident effect on the solid beam response as shown in figure 4.10.

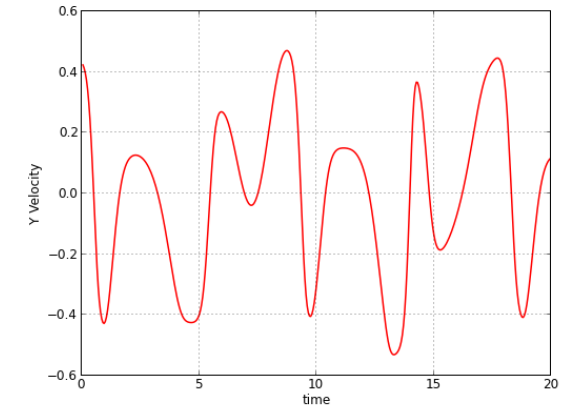

(a)

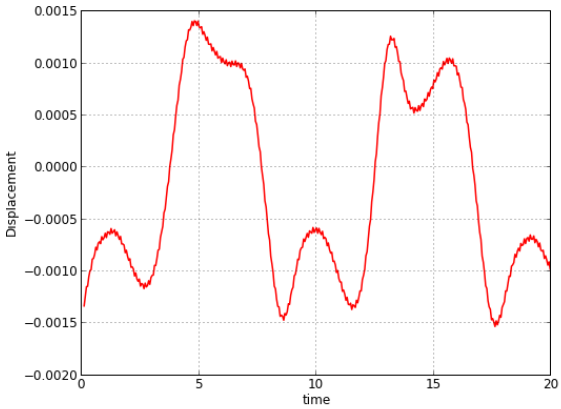

(b)

Figure 4.10: figure 4.10a Y velocity for fluid at point $8.3, 2)$, figure 4.10b displacement for point $(7.99, 2)$

It can be seen that the displacement of the beam follows the same shape as the Y velocity although out of phase. This is expected as the same point can not be plotted both for fluid and solid and the solution takes more time to get to the fluid sampling point than to the solid tip. On the other hand it can be seen that the velocity undergoes larger changes across time hinting that higher frequency modes are present, modes that the beam, with a higher mass and inertia, cannot

reproduce.

Results are not compared with the ones obtained in [7] as non linear elasticity is not reproduced in this project, this is left as a short term objective from the finalization of this work.

5 REDUCED ORDER MODELS

Proper Orthogonal Decomposition (POD) Reduced Order Models (ROM) consist on projecting a full order solution (FOM) into low dimensional spaces of solutions. The underlying idea is actually simple; it relies on the decomposition of the FOM into its most important or representative components. It can be thought of as obtaining the main frequencies of a signal and then through these reproducing either the same initial signal or similar ones with certain precision.

As a developing subject of research there are still problems to solve. When the solution is projected into the reduced dimensional space the components that are not projected will not be taken into account when solving the reduced model. With some degree of abstraction it can be seen that this is precisely the same problem faced with the Navier-Stokes equations with highly convective flows that was mentioned earlier. When the element used cannot reproduce on its enterity the whole behaviour of the solution stabilization is needed. In other words the element doesn't capture the high frequency component of the solution so additional input from the subgrid scale is added. In fact in [2] a novel approach is discussed where the non present component of the FOM is added through the subgrid scales after the decomposition has been made.

5.1 SOME ROM THEORY

Let us define a vector field $\mathbf{U} \in R^M$ and the full order space $\mathcal{V} = R^M$ where M represents the dimension of the unknown and is associated with the number of nodes of the used mesh. The non linear, transient, fully discretized problem is,

$$A(U^{n+1})U^{n+1} = R(U^n, U^{n-1}, \cdots), \tag{5–1}$$

Where n is the timestep counter, A is the system matrix which might depend on U^{n+1} and R is the right hand side which might also depend on the unkown.

The solution to this system can be projected into a low dimensional space in the following way,

$$\mathbf{U} \approx \Phi \mathbf{U}_\Phi \tag{5–2}$$

Where $\Phi \subset R^{M \times m}$ is an orthonormal base to this new space of solutions, $\mathcal{V}_\Phi \subset R^M$, where m is the dimension of the new low dimensional space. $\mathbf{U}_\Phi \in R^m$ are the components of the solution in the new space.

It is convenient to express the solution as a sum of the mean and reduced order representation,

$$\mathbf{U} \approx \Phi \mathbf{U}_\Phi + \overline{U} \tag{5–3}$$

As will be shown later the precision of the results depend greatly on the base calculated. There are many ways to obtain this base, but in the development of this project only Proper Orthogonal Decomposition was used. Then, introducing equation 5–3 into equation 5–1 leads to an overdetermined system as follows,

$$A\mathbf{U}_\Phi = R - A\overline{U} \tag{5–4}$$

If the A matrix is positive definite and symmetric a least-squares Galerkin strategy can be used to approximate the overdetermined system as,

$$\Phi_T A \Phi \mathbf{U}_\Phi = \Phi_T R - \Phi_T A \overline{U} \tag{5–5}$$

Now, introducing the following notation,

$$A_\Phi := \Phi_T A \Phi \in R^{m \times m} \tag{5–6}$$

$$R_\Phi := \Phi_T (R - A\overline{U}) \in R^m \tag{5–7}$$

The reduced system can be expressed as,

$$A_\Phi U_\Phi^{n+1} = R_\Phi, \tag{5–8}$$

An algebraic system that has a many degrees of freedom as the base, which is, tipically much less that the original full order model.

5.2 A REVIEW OF POD

The final step towards an understanding of the underlying ideas of reduced order modeling is calculating the reduced order basis Φ. The processed can be summirized as follows, first a series of snapshots of the solution of the FOM are stored to then apply a Singular Value Decomposition (SVD) and finally obtain the most important basis functions.

The snapshot matrix is defined as:

$$\mathcal{U} \in \mathrm{R}^{M \times N} \tag{5–9}$$

Where N is the number of snapshots. Each column of $\mathcal{U}$ corresponds to a snapshot of the solution of the FOM. In the cases explained later each one of this columns corresponds to a solution of the whole system for each selected time step. Of course the more snapshots that can be obtained the more data the reduced system will have to display a more approximate solution.

This matrix will the be decomposed into the addition of a mean value matrix and a product of three matrices in a process called Singular Value Decomposition, in the following way,

$$\mathcal{U} = \overline{\mathcal{U}} + \Phi_0 \Sigma_0 \Psi_0^T \tag{5–10}$$

Where $\Phi_0 \in \mathrm{R}^{M \times M}$ is a basis for R^M. $\Sigma_0 \in \mathrm{R}^{M \times N}$ is the eigenvalue matrix and $\Psi_0^T \in \mathrm{R}^{N \times N}$ is the representation of the snapshots in the new basis.

This SVD decomposition has the following properties:

- Φ_0 is an othogonal matrix, which means that its product by it transpose is the identity matrix, where the first $N_0 \leqslant N$ columns can reproduce exactly the snapshots contained in the matrix $\mathcal{U}$
- Σ_0 is a diagonal matrix which contains, from greatest to least, the eigenvalues of the associated basis functions. The ordering of the eigenvalues is a measure of the relative importance of each of the basis functions in the whole system.
- Ψ_0 is an orthogonal matrix containing the projection of the snapshots into the new basis.

Knowing that the eigenvalues decrease in value very quickly one can choose the first m eigenvalues to get an approximation to the solution of the problem. Where m can be very small compared to the total number of eigenvalues. At this point the power of reduced order modeling can be appreciated. If m is sufficiently small, the time to compute the reduced system is minimal. The set of snapshots can be approximated as,

$$\mathcal{U} - \overline{\mathcal{U}} \approx \Phi \Sigma \Psi^T \tag{5–11}$$

Where the projected snapshots $\Sigma\Psi^T$ can be denoted as $\mathcal{U}_\Phi$. Finally the solution can be expressed as,

$$\mathcal{U}_\Phi = \Phi^T(\mathcal{U} - \overline{\mathcal{U}}) \tag{5–12}$$

5.3 NUMERICAL EXAMPLES

In the following sections numerical examples of solid, fluid and FSI will be displayed. The idea is to show the power, as well as some difficulties, of ROM. In this sense it is worth noting that all results were obtained with a preliminary version of the code and there still remains a lot to be done to achieve the expected performance in some cases. During the development of this cases it was seen that by applying a methodology, succesfull ROM simulations could be obtained. The course of action was the following,

- Reach a stationary state of the FOM, in simple cases, as linear elasticity, this proved to be not important
- Make a Fourier transform of one point of the domain were the quantities vary noticeably

- From the obtained spectrum obtain the most important frequencies
- Run ROM case in offline mode taking sufficient number of snapshots (depends on case complexity)
- Run ROM case using the number of modes obtained from Fourier transform

In all cases, using this methodology proved to provide accurate results as will be shown in the examples. It important to remark that all of the analyzed cases are of dynamic nature so that is the reason why the Fourier transform is proposed as part of the methodology. ROM should not be associated only to dynamic cases but to any kind system in which there is a varying quantity.

The cases to be reproduced are modified versions of the cases that were benchmarked in previous sections for each topic.

5.3.1 Solid - Rom

The following example illustrates the oscillation of a cantiliver elastic beam, the previous methodology is specially didactic in this case as, by using increasing number of basis vectors the relative importance of each eigenvalue is seen.

Figure 5.1 shows the mesh used for this particular case composed of 100 bilinear quadrilaterals. The properties are shown in table 5.1.

Young's modulus	7850
Poisson's modulus	0.0
Length	1.0
Thickness	0.05

Table 5.1: Material properties and geometry of beam

Figure 5.1: Meshed beam,# elements = 100

The analytical first mode of the bar, calculated from 2–14 is found to be 20 Hz. Figure 5.2 shows the Fourier transform of the displacement of the tip of the beam. As it can be seen the first mode has been approximated quite well, the idea is that the ROM case replicates this result, with less computational cost.

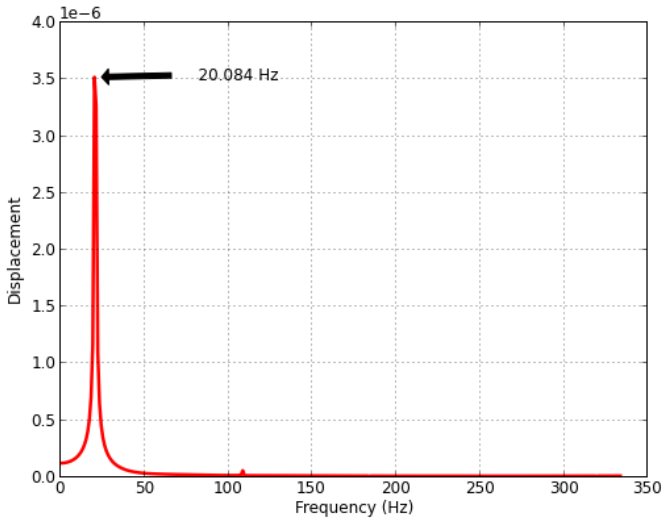

Figure 5.2: Full order model

Table 5.2 shows the parameters used to run the ROM case. From the solved system 3 main eigenvalues where found, and as it was expected their value decrease quite rapidly.

# of snapshots	2
size of calculated base	3

Table 5.2: Important ROM parameters

Figure 5.3 shows the case where from the calculated base from the FOM case only the main eigenvalue and its corresponding base was used to reproduce the case. As it can be seen the result can reproduce exactly the main frequency, which is the one with highest energy, but the other harmonics do not appear on the solution, as it is expected as there is no information to be able to produce this data.

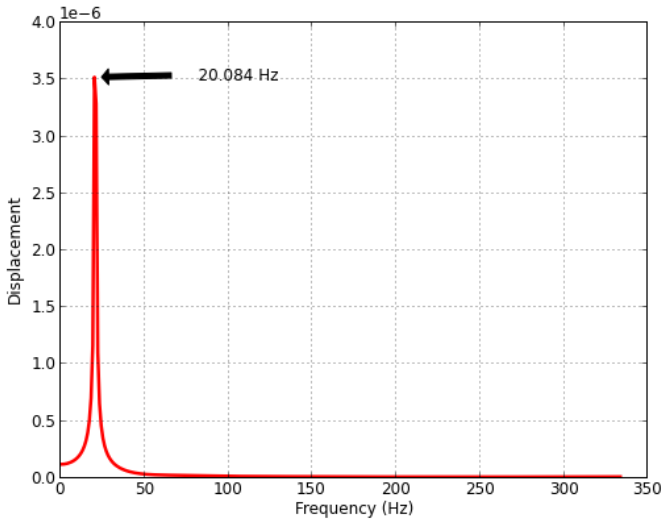

Figure 5.3: ROM, # modes = 1

In figure 5.4 one more eigenvalue and base were added, it can be seen that around 110 Hz a second harmonic starts to appear. While the frequency of the harmonic is the correct one the energy associated to it is lower that in the FOM result.

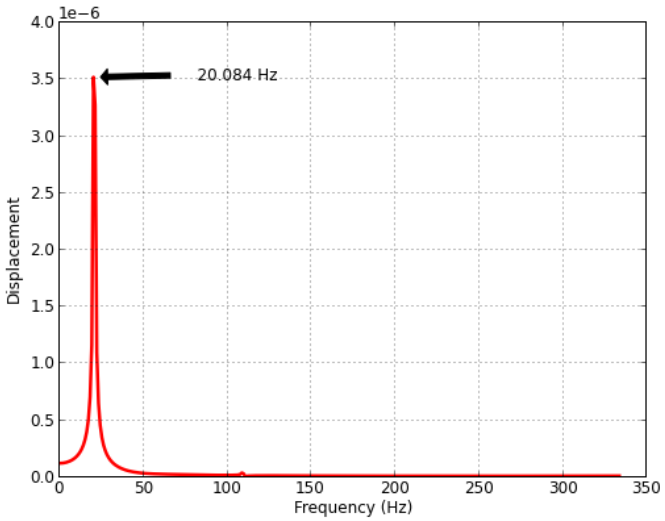

Figure 5.4: ROM, # modes = 2

Finally, on figure 5.5, all three calculated eigenvalues and basis vectors are used to calculate the solution. As it can be seen the solution was reproduced exactly.

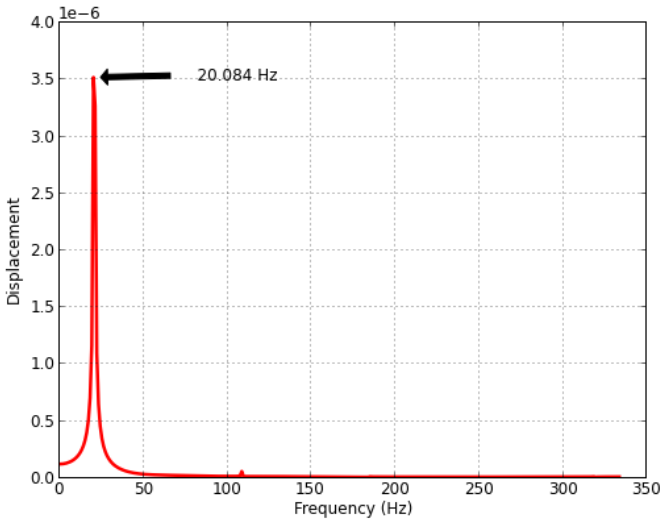

Figure 5.5: ROM, # modes = 3

Table 5.3 shows the time and computational cost comparison for the FOM and ROM cases.

Solution times

	FOM	ROM	ROM	ROM
Size of basis		1	2	3
solution time (s)	5.03	1.67	1.665	1.54
solution time speed up (%)	-	66.8	66.89	69.38

Table 5.3: Comparison of FOM - ROM solution times

As it can be seen the speed up for the linear elastic case is in the worst case 66.8% which is a considerable time save as the case is extremely simple and FOM solution itself took only 5 seconds to calculate.

5.3.2 Fluid - Rom

While the linear solid elastic case was reproduced with no problem and exactly with no difficulty sadly the case for the fluid proves to be quite different as the physics associated to the flow is much more complex and non linear. To be able to run a case succesfully with the ROM the initial transitory part of the evolution of the flow had to be ignored from the sampling. It is possible that the evolution of the flow during this period carries many frequencies that will dissapear over time or that will be dampened once the flow becomes developed and statistically stationary. When ROM was attempted during this stage the base recovered from the eigensolver could not reproduce the FOM succesfully.

Once this difficulty was overcome the flow around a cylinder was used to study ROM on fluids. Physical properties and parameters are shown in table 5.4.

Cylinder diameter	$d = 0.4$
Center of cylinder	$X_c = 0.8, Y_c = 1.2$
Channel length	$L = 7.0$
Density of fluid	1
Viscosity of fluid	$1e-4$

Table 5.4: Material properties and parameter of case

The geometry of the case is shown in figure 5.6 .

Figure 5.6: Geometry of test case

Boundary conditions for the domain are shown in table 5.5.

Domain	Fluid
$x = 0$	$vel_x = 1, vel_y = 0.0$
$x = 7$	$vel_x = vel_y = \text{Free}$
$y = 0 = 2.4$	$vel_x = free, vel_y = 0$
cylinder surface	$vel_x = vel_y = 0$

Table 5.5: Boundary conditions

Parameters for the ROM run during offline phase are shown in table 5.6

# of snapshots	100
size of calculated base	10

Table 5.6: Important ROM parameters

Mesh

Figure 5.7 shows the mesh used to run all cases, notice the refinement made surrounding the cylinder to be able to capture the boundary layer of the flow correctly.

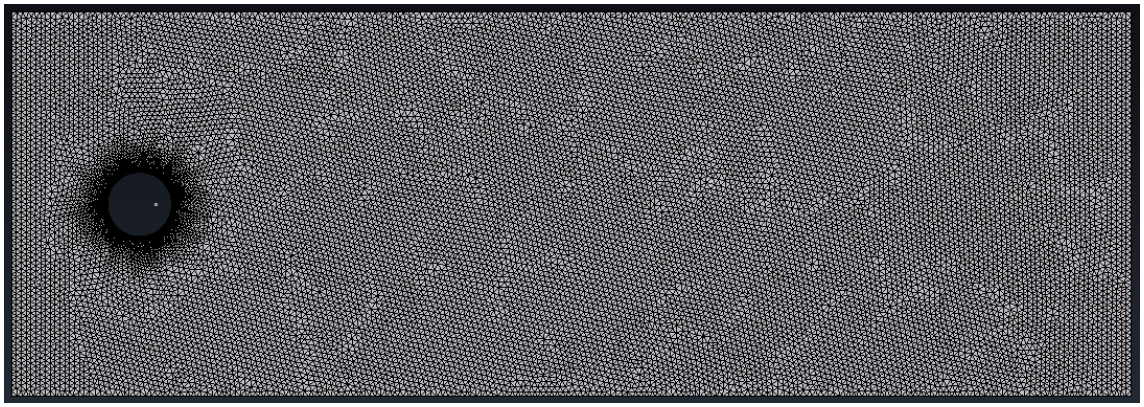

Figure 5.7: Mesh of test case

The properties of the mesh are shown in table 5.7.

Domain	Fluid
Element	Linear Tri
# Elements	36186
# Nodes	18487

Table 5.7: Mesh properties

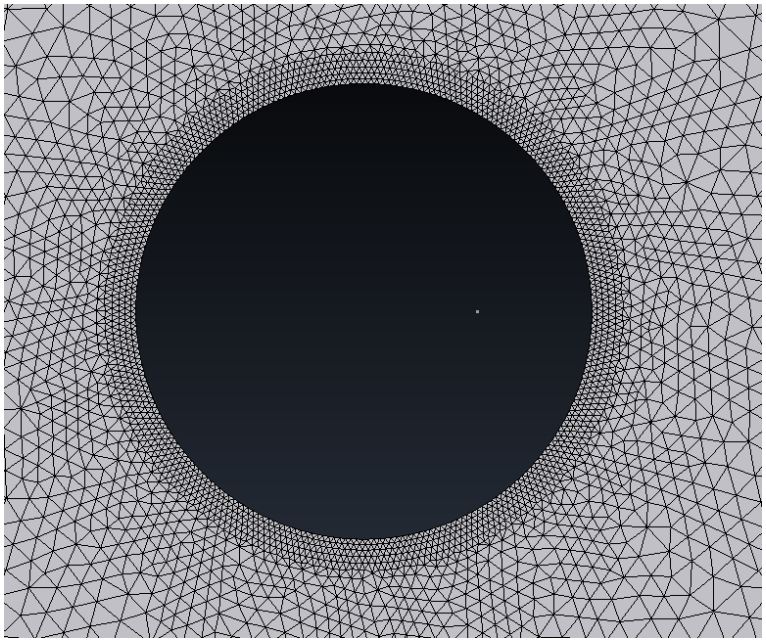

Figure 5.8: Mesh around the cylinder

Results

Results will be analyzed for velocity and pressure for the FOM and for a ROM approximation using 3 basis vectors. From the POD decompositon a base of 10 eigenvalues was obtained where the first three were the ones with the highest energy. The rest decreased rapidly and therefore could, for experimental purposes, be discarded. It was found that by using the first seven basis vectors the solution had little difference from the FOM, so to be able to appreciate some difference, and from this, the full power of ROMs it seemed like a proper choice to compare against 3 basis vectors.

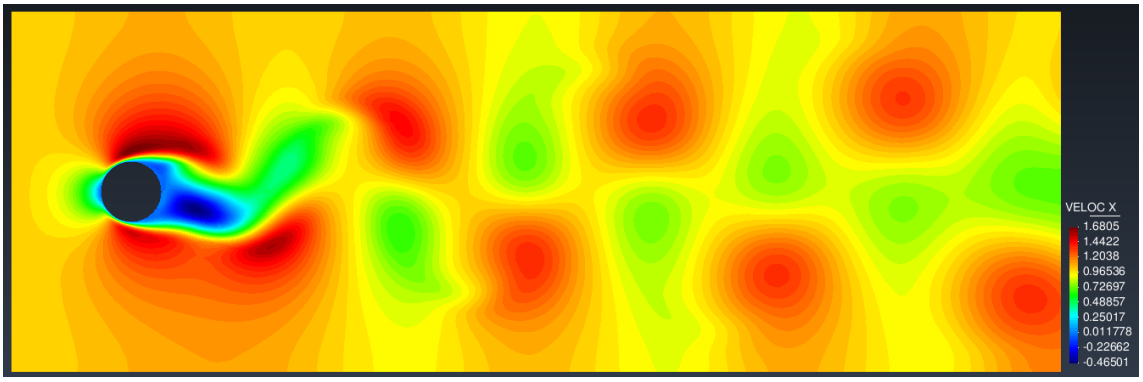

Figure 5.9: velocity X for FOM

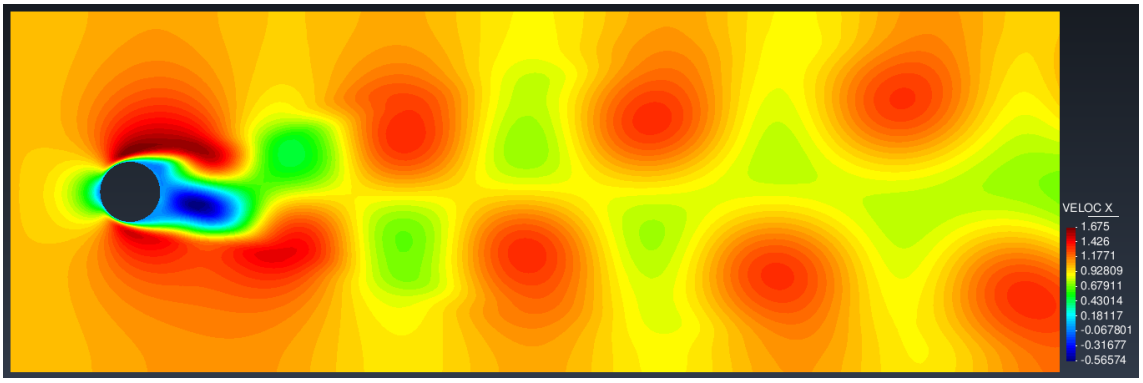

Figure 5.10: velocity X for ROM, 3 basis vectors used

It can be seen from figures 5.9 and 5.10 that by using the first three modes the solution appears to be very similar to the FOM but with some degree of added diffusion in the solution for the x component of the velocity. This can further be seen by the decreased magnitude of the results.

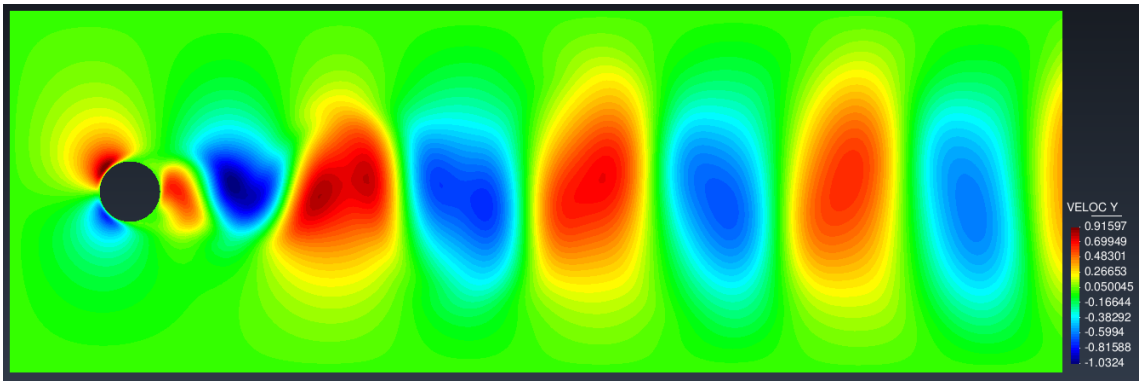

Figure 5.11: velocity Y for FOM

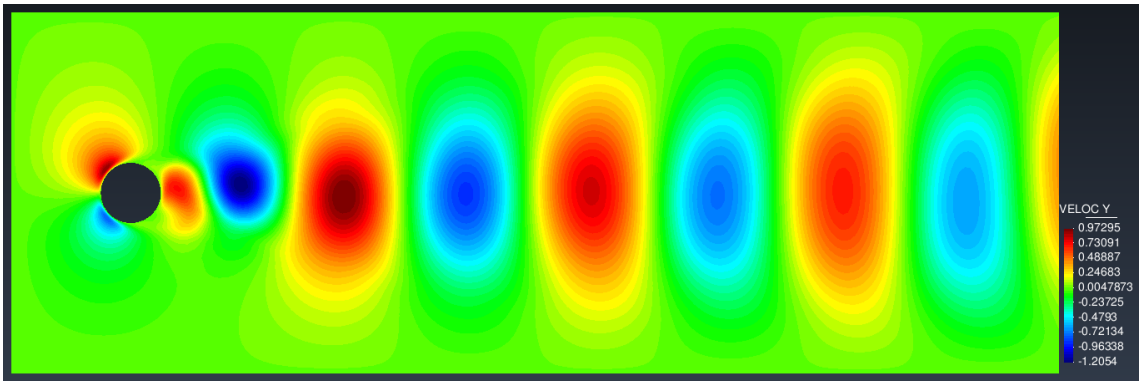

Figure 5.12: velocity Y for ROM, 3 basis vectors used

Unlike the previous case, figures 5.11 and 5.12 show an amplified solution and a higher intensity of the vortex that the cylinder sheds through time. Also the 'bubbles' appear to be more symmetrical in ROM than in the FOM counterpart. Probably the lower modes decrease the symmetry of the solution.

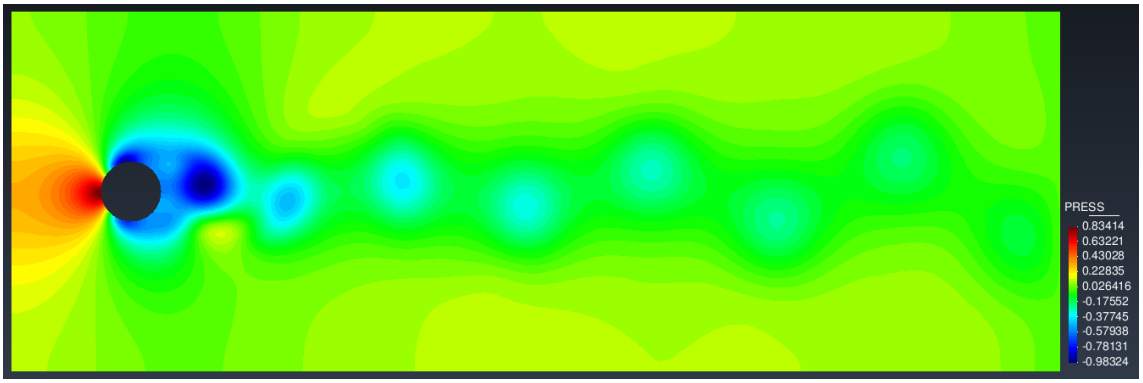

Figure 5.13: Pressure for FOM

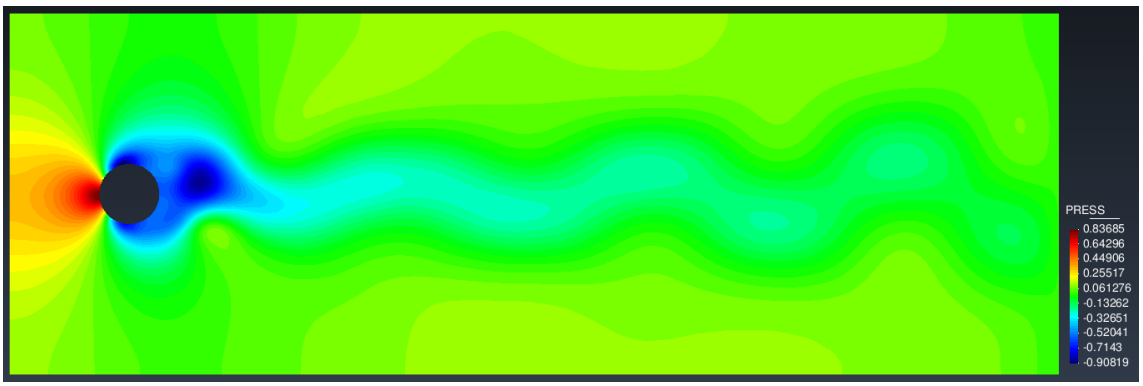

Figure 5.14: Pressure for ROM, 3 basis vectors used

The results shown in figures 5.13 and 5.14 are quite interesting as they are similar in magnitude but differ in the numerical phenomena that carries the solution through time. While in the ROM case the cylinder sheds pressure bubbles, accounting for the vortex shedding of the previous cases, in the ROM case the pressure is dissipated continously in a oscillatory manner.

Finally, in figure 5.15, the y velocity was plotted for point (1.3,0) just behind the cylinders geometry. It can be seen how each added mode interacts in such a way to approximate in a better manner the solution until when it is barely noticeable the difference between ROM and FOM.

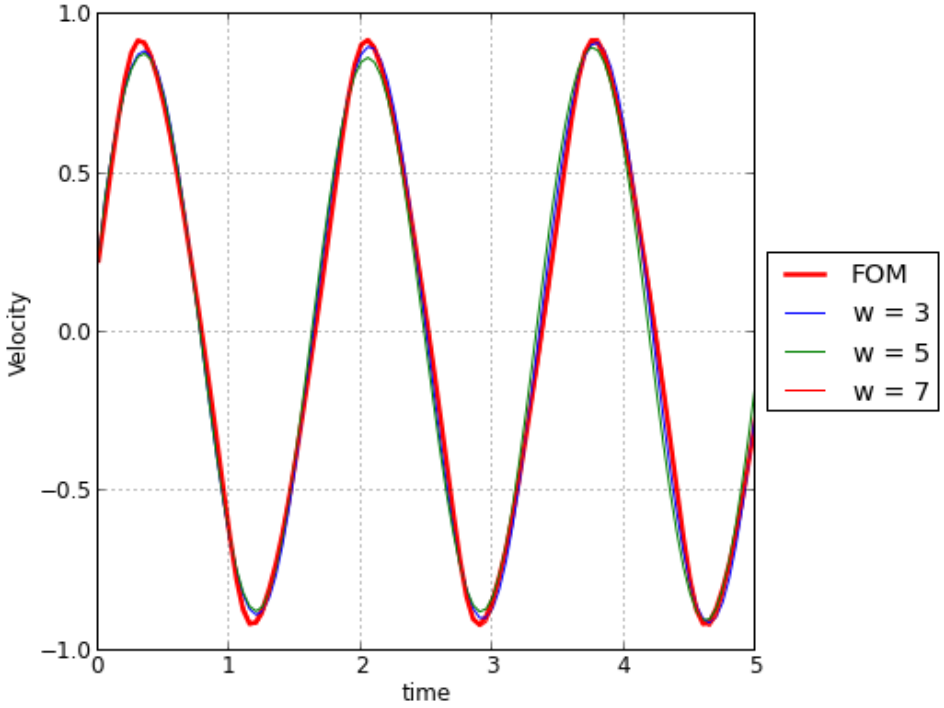

Figure 5.15: Velocity in Y for point (1.3,0)

Solution times

	FOM	ROM	ROM	ROM
Size of basis		3	5	10
solution time (s)	687.843	20.049	18.25	18.18
solution time speed up (%)	-	90.28	97.34	97.35

Table 5.8: Comparison of FOM - ROM solution times

It is interesting to see how the speed up of the solution is much higher than the previous solid elastic case. This is expected though as the phenomena is much

more complex and the FOM solution takes much more time too compute. It is also worth noting that as the number of basis vectors increases the speed up does as well. This can be due to a much better representation of the solution and in turn faster convergence to the FOM solution.

5.3.3 FSI - Rom

Finally the main objective of the proyect, fluid structure interaction approximated using ROM, was tackled using as test case the turek benchmark shown in chapter 4. For this test case the same geometry, mesh and boundary conditions were used. The ROM parameters are shown in table 5.9.

# of snapshots	600
size of calculated base	50

Table 5.9: Important ROM parameters

In the following sections results will be shown for fluid and solid separately. In the same manner as in the flow past a cylinder rom benchmark, see section 5.3.2, results are shown compared to their ROM counterpart with increasing number of modes.

This case proved to be much more complex than the previous ones as the flow is more involved and obtaining a stationary state involved a lot of computational time. The results, then, are regarded as preliminary as more study has to be done to properly characterize this case and represent it. The main idea and approximate results are obtained.

Fourier transform of FOM solution

Before running the ROM cases a Fourier transform was done for the tip displacement of the beam and a for a point in the fluid domain near the tip, see figures 5.16 and 5.17 to get a notion of the principal frequencies acting on this particular problem. The results were used to choose the number of eigenvalues and eigenvectors used for the ROM computations. This is an important decision as the objective is to reduce dramatically solution time by having a sufficiently small base. The only inconvenience being that if the chosen base is not representative enough important modes of the full order solution maybe lost as was shown in solid ROM benchmarking, see section 5.3.1 where this is exemplified.

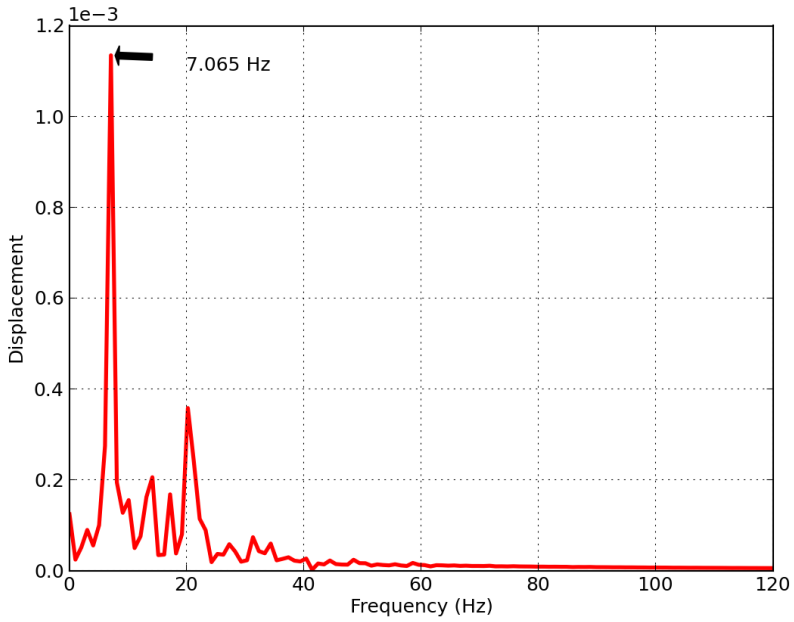

Figure 5.16: FFT of displacement Y at $(7.99, 2)$

From figure 5.16 around 7 main modes can be seen.

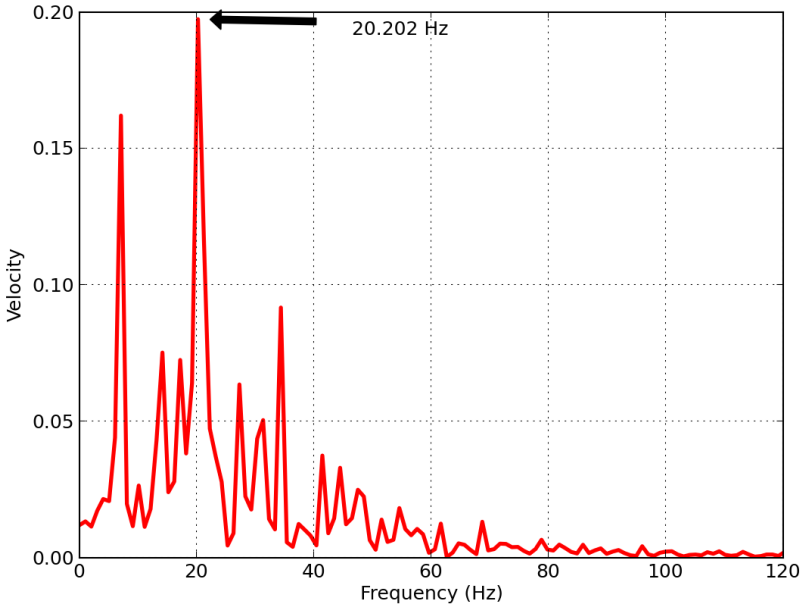

Figure 5.17: FFT of velocity Y at $(8.3, 2)$

From figure 5.17 around 20 main modes can be seen, it is worth noting that it is not a coincidence that the most energetic modes in figures 5.16 and 5.17 are the same ones as the solution is coupled. In this particular case, as the solid is not influencing fluid movement, the fluid drives the motion. The principal modes are around 7Hz and 20.2Hz. It is most interesting to see that as the solid cannot react inmmediately to the highest frequencies of the fluid, it is mostly affected by the lower continous modes, reason why even though the 20.2Hz mode is the most energetic one in the fluid flow, in the solid it is the 7Hz one.

Results for cantiliver beam

As it was mentioned, the fluid is the one driving the motion as the assumption is that the solid is linearly elastic, so its influence is minimal in the flow. All ROM solution were run using 7 modes and for different values of fluid modes.

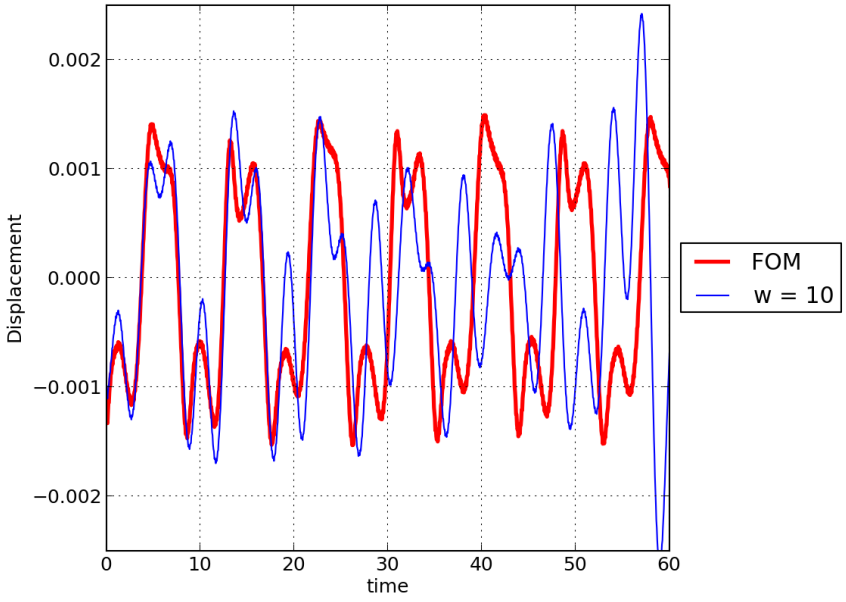

Figure 5.18: Comparison between FOM and ROM using 10 modes for displacement Y at $(7.99, 2)$

As it can be seen from figure 5.18 the ROM solution appears to have amplitude problems, and after the first 30 seconds, important phase disorders. After 50 seconds it can be seen how the approximated solution starts to oscillate strongly. It can be seen how this solution is not approximated satisfactorily with so little amount of modes.

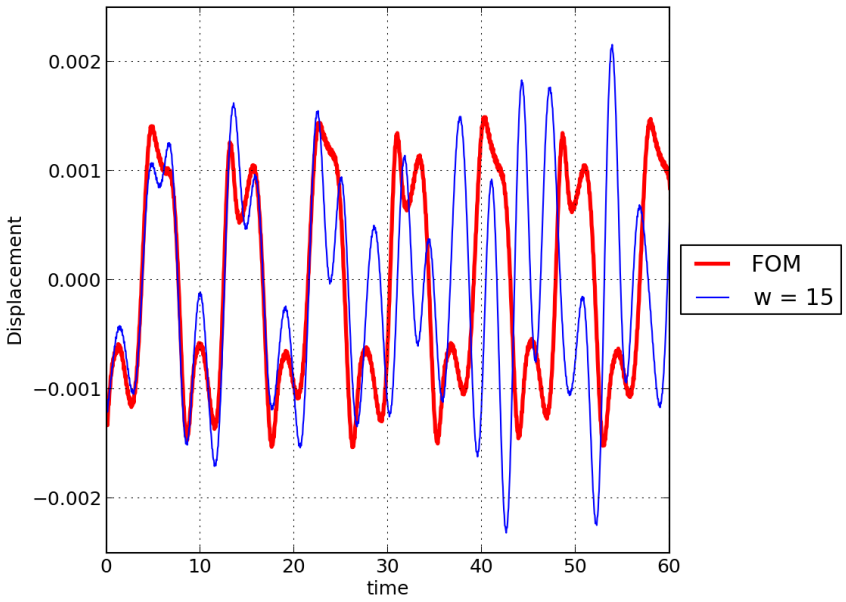

Figure 5.19: Comparison between FOM and ROM using 15 modes for displacement Y at $(7.99, 2)$

Figures 5.18 and 5.19 show similar results. It can be seen how the amplification moved from 50 seconds to 40 seconds. This solution again produces non feasible results after the first 30 seconds.

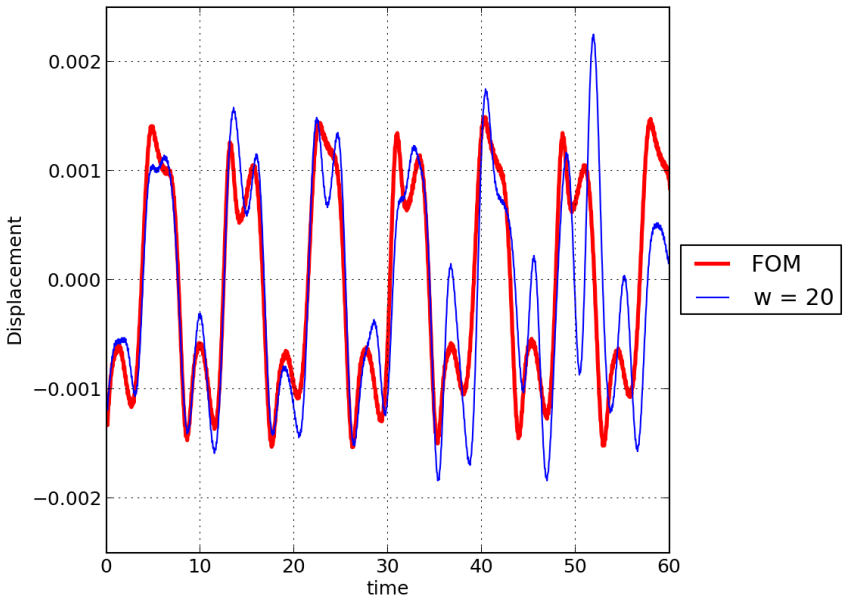

Figure 5.20: Comparison between FOM and ROM using 20 modes for displacement Y at $(7.99, 2)$

From figure 5.20 it can be seen how by using 20 modes the phase problems have been corrected notoriously as well as the amplitude issues. There remains some problems with the amplitude of the solution and some modes are not being reproduced at all, see figure 5.20 at around 23 seconds. This will be discussed in later sections.

Results for fluid flow

From figure 5.21 it can be seen how after the first 30 seconds the solution begins to present amplitude and phase problems, much like in the associated solid case.

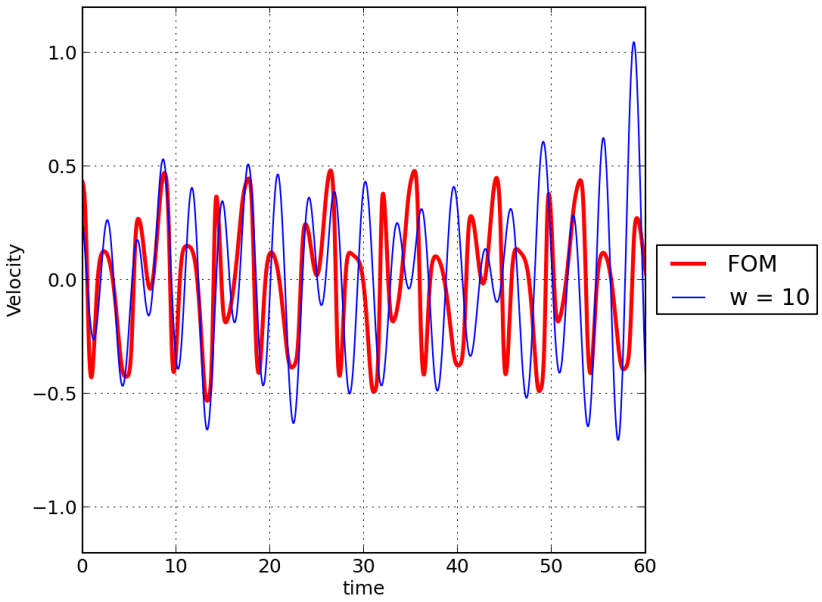

Figure 5.21: Comparison between FOM and ROM using 10 modes for velocity Y at $(8.3, 2)$

Figures 5.21 and 5.22 present, once again similar behavior. It appears that by adding 5 more modes the solution is better approximated for the first 30 seconds. Afterwards the solution becomes polluted and spurious oscillations appear.

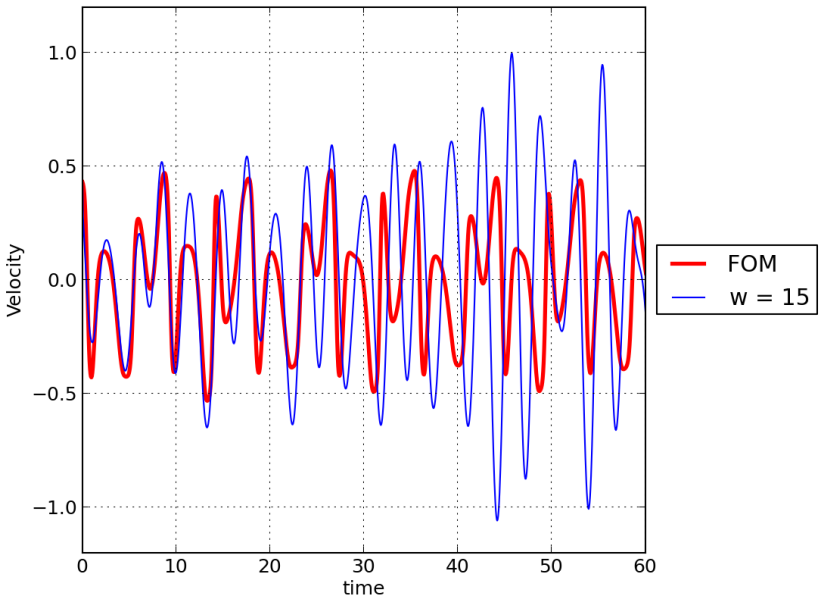

Figure 5.22: Comparison between FOM and ROM using 15 modes for velocity Y at $(8.3, 2)$

Similarly to the associated solid case figure 5.23 presents a much better approximation of the solution even though some amplifications and phase issues still persist.

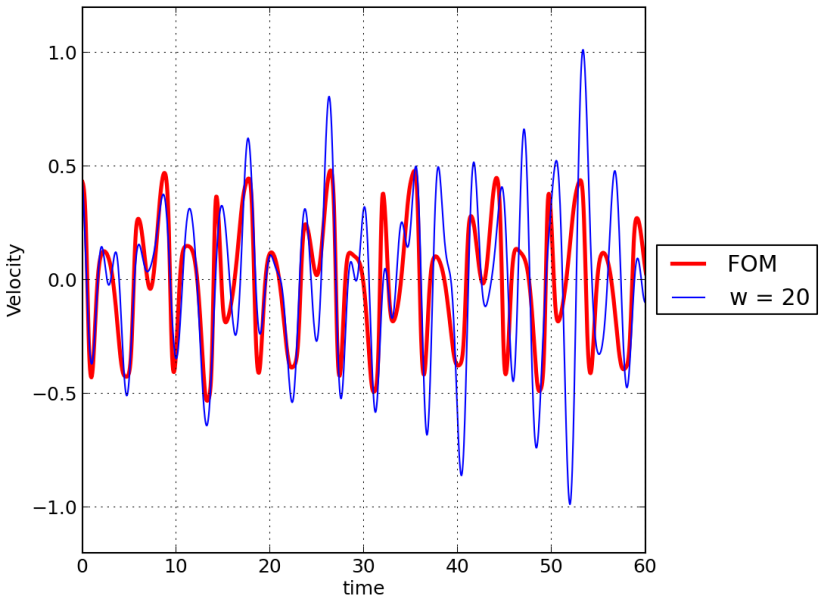

Figure 5.23: Comparison between FOM and ROM using 20 modes for velocity Y at $(8.3, 2)$

It can be seen that neither solid or fluid converged as closely as in the previous cases to the FOM solution. In the following sections this will be discussed.

Velocity contours

In the following figures the contour plots of velocities and pressure are shown to better exemplify what the previous plots show. It is interesting to see that adding more modes removes spurious oscillations and in turn converges more closely to the FOM solution.

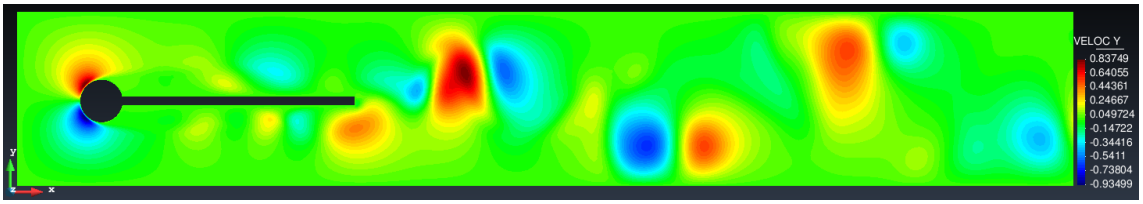

Figure 5.24: Velocity magnitude for FOM

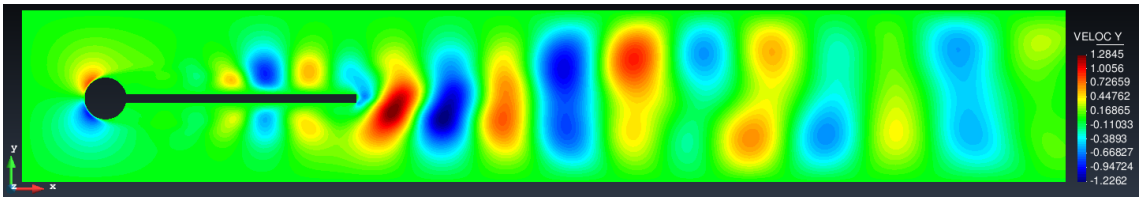

Figure 5.25: Velocity magnitude for ROM using 10 modes

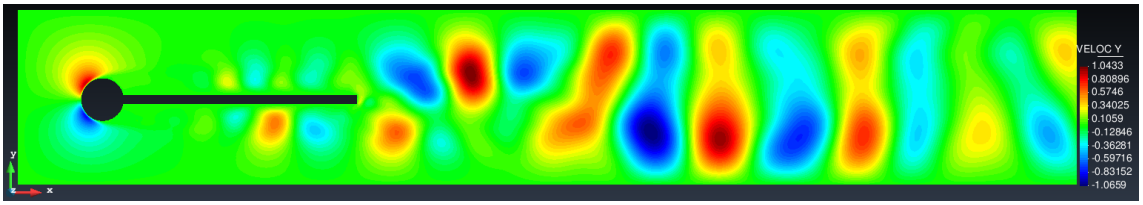

Figure 5.26: Velocity magnitude for ROM using 20 modes

Pressure contours

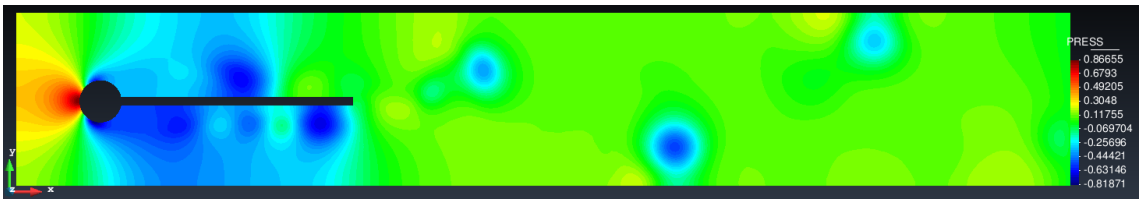

Figure 5.27: Velocity magnitude for FOM

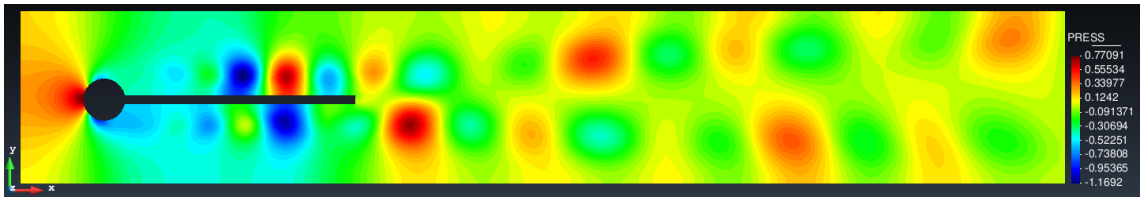

Figure 5.28: Pressure for ROM using 10 modes

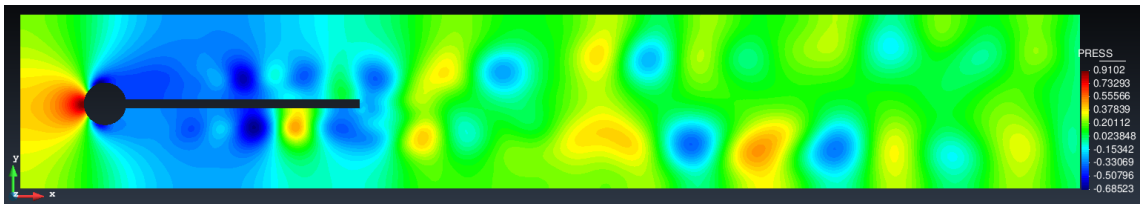

Figure 5.29: Pressure for ROM using 20 modes

Solution times

	FOM	ROM	ROM	ROM
Size of basis		10	15	20
solution time (s)	7,838.9	6,541.8	7,000.0	7,689.9
solution time speed up (%)	-	16.54	10.70	1.90

Table 5.10: Comparison of FOM - ROM solution times

It is clear from table 5.10 that for a much more complex problem were a great number of degrees of freedom are involved the speed up is not that dramatic as was seen in sections 5.3.1 and 5.3.2. As it will be pointed out in the next section this decrease in speed up can be due to a great variety of reasons, but as a first approach with the simplest of iterative by sub domain couplings this is considered quite a success.

General discussion

The effect of using varying amount of modes was seen in the previous sections and it is worth noting that even though the solution for 10 modes presents oscillations, amplifications and phase disorders. It can actually approximate the first 30 seconds quite similarly to the other case which used more modes and took longer solve time. This issue remains to be solved as it can be due to various factors which by time reasons were not explored like, taking more snapshots during the build phase of the ROM module, increasing convergence of the linear solver of the ROM module, changing time step size.

Due to time constraints only the mentioned Galerkin proyection of the system was explored. It is a possibility that by using a Petrov-Galerkin approach the calculated ROM solution would fall within an expected converged tolerance. This is left as a short term objective.

The flow present in this case is quite complicated and the fact that the bar appears to be rigid to the fluid creates complicated flow patterns that exhibit symmetry over large periods of time, which for the present case is around 20 seconds. This coupled with the fast energetic modes makes the associated base calculated by the SVD quite large. A good approximation was obtained for up to 20 modes with lower solution time compared to the FOM problem. After this time started to be similar and, if the whole base was used, the solution took longer than the FOM, which made the analysis, aside from purely didactic, useless.

Most of the computational time during the ROM run was used to project the reduced solution back to the full order space,

$$\mathcal{U} = \Phi \mathcal{U}_\Phi \tag{5–13}$$

It is worth noting that if the problem is large the dimension of the base can get quite large as well and the solution time of equation 5–13, even though it is just a mulitplication, can be actually costly in terms of computational time, specially if the code is not fully optimized, this is, using fully vectorized operations and reduced cycle control like if and switch statements.

6 THE CODE

All cases were run using FEMUSS, Finite Element Methods Using Subgrid Scale, a code developed currently at CIMNE. FEMUSS, running on FORTRAN is conceived as modular code adapted to run different kinds of physical problems. Currently FEMUSS can solve fluid flow problems of low viscosity turbulent flows, highly viscous fluids, highly compressible flows, near Mach number flows as well as acoustic and wave propagation scenarios and as of this project solid elastodynamics and the corresponding coupling between Fluid and Solid modules to achieve FSI with ROM. As any conventional numerical simulation code FEMUSS relies upon a master driver to control program execution, from initializations, module iteration, convergence calculation to program termination.

For the development of this project the added input into the code was the addition of the Solids module which up to this point only solves linear elasticity but it expected to expand to non linear in the short term. As it was seen, the coupling between domains can be relatively straightforward, for the simplest of cases, but in reality its implementation poses some problems. The first of which is how to achieve proper information transfer between physics or, in this case physical problem modules, specially, as it was the case, when one of the domains requires much less degrees of freedom than the other one and uses non conforming meshes.

To solve this complication an abstraction of the master driver was done as well

as design of a container class which enables the code to instance dynamically each module and most importantly each case to be solved. The idea was to treat each module as a separate case which by use of a communicator class that can send data, and if necessary, interpolate it to deal with possible non conforming meshes.

The following diagram exemplifies the mentioned concepts with hope that it will break down a little bit the abstraction.

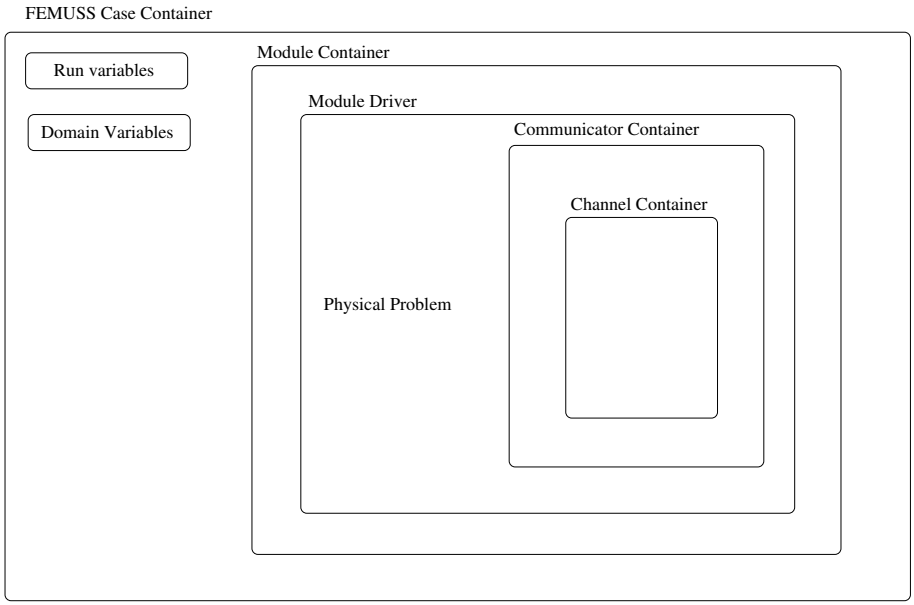

Figure 6.1: Container scheme

As it can be seen from figure 6.1 each case is composed of a series of container objects and some local case variables that control the run. The most important aspect of this implementation is the new capabilites between modules to share information and if necessary to process it. This can be better understood from figure 6.2 where a hypothetical case is run. In this problem a fluid-temperature structure interaction problem is going to be solved. For this case a series of communicators are set up as shown.

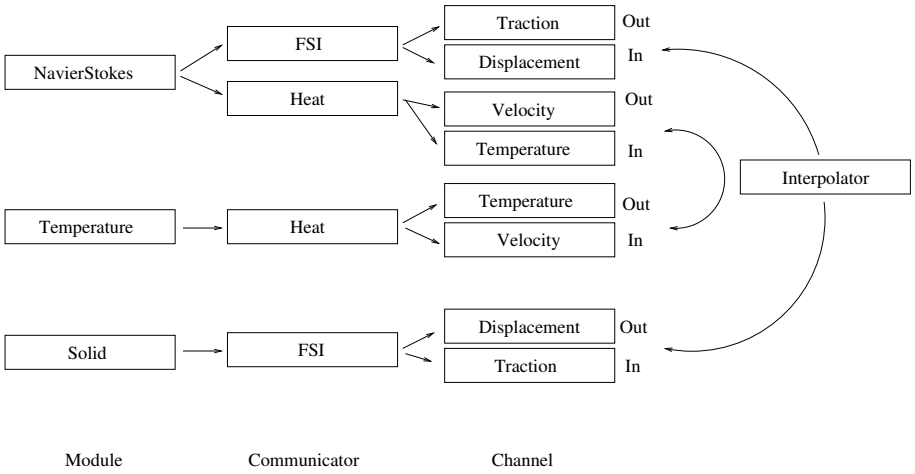

Figure 6.2: Communicator scheme of each container

The idea is that while the NavierStokes and Temperature module run in the same mesh, the Solid module runs with another one, note that it has be assumed that the Solid is not affected by thermal effects, just the fluid. This makes it necessary to interpolate the information when transfering data. With the mentioned implementation, using communicators and channels, this is readily done as the output is interpolated before reaching its destination.

From the programming point of view, each of this containers is a linked list that can be iterated in any direction. The core of this link list is an unlimited polymorphism pointer that allows storage of any kind of data. With this the linked list, termed as container, can store any collection of data and iterate through it. It is the same concept of template in C++.

BIBLIOGRAPHY

[1] Joan Baiges Aznar. "The Fixed-Mesh ALE method applied to multiphysics problems using stabilized formulations". In: *Materia (s)* 14.December (2011), pp. 01–2011.

[2] Joan Baiges, Ramon Codina, and Sergio Idelsohn. "Reduced-Order Subscales for POD models". In: (2014), pp. 1–27.

[3] M. Cervera, M. Chiumenti, and R. Codina. "Mixed Stabilized Finite Element Methods in Nonlinear Solid Mechanics . Part I : Formulation". In: ().

[4] Ramon Codina. "Analysis of a stabilized finite element approximation of the Oseen equations using orthogonal subscales". In: *Applied Numerical Mathematics* 58.3 (2008), pp. 264–283. ISSN: 01689274. DOI: 10.1016/j.apnum.2006.11.011.

[5] Ramon Codina. "Stabilization of incompressibility and convection through orthogonal sub-scales in finite element methods". In: *Computer Methods in Applied Mechanics and Engineering* 190.13-14 (2000), pp. 1579–1599. ISSN: 00457825. DOI: 10.1016/S0045-7825(00)00254-1.

[6] Ramon Codina et al. "Time dependent subscales in the stabilized finite element approximation of incompressible flow problems". In: *Computer Methods in Applied Mechanics and Engineering* 196.21-24 (2007), pp. 2413–2430. ISSN: 00457825. DOI: 10.1016/j.cma.2007.01.002.

[7] Jaroslav Hron and Stefan Turek. "Proposal for numerical benchmarking of fluid-structure interaction between an elastic object and laminar incompressible flow". In: *Fluid-Structure Interaction* 53 (2006), pp. 371–385. ISSN: 14397358. DOI: 10.1007/3-540-34596-5_15.

[8] Thomas J.R. Hughes et al. "The variational multiscale method—a paradigm for computational mechanics". In: *Computer Methods in Applied Mechanics and Engineering* 166.1-2 (1998), pp. 3–24. ISSN: 00457825. DOI: 10.1016/S0045-7825(98)00079-6.

[9] University Of Manchester OOMPH.lib. *http://oomph-lib.maths.man.ac.uk/doc/interaction/turek_* 2015.

[10] Singiresu S Rao. *Vibration of Continuous Systems*. John Wiley & Sons, Inc, 2007. ISBN: 9780471771715.

[11] Cory Rupp, Micah Howard, and Gary Weickum. "Incompressible Mixed (u / p) Elements for the CAS FEM Code". In: (), pp. 1–10.